Università degli studi di Padova
Tesi di laurea in Fisica
Anno accademico 2008/2009

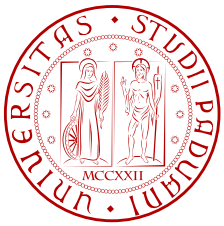

Coarse Grained Model of a Nanoparticle Inclusion in a Bilayer Membrane

Relatore: A. Maritan
Correlatore: M. Müller

Laureando: G. Marelli

Contents

List of Figures

Introduction

Loading cells with magnetic nanoparticles has become an essential tool to treat diseases by transporting a drug into a particular tissue [Drummond DC et al. 1999], [Papahadjopoulos D et al.1991], for chemotherapy [P. R. Mishra (2003)],[Dass *et al.* (2000)],[Singh *et al.* (1996)],[Sarkar and Yang (2008)] and for the development of new imaging techniques [Kim *et al.* (2007)], [Kelly *et al.* (2008)]. The insertion of an external entity into a biological cell is experimentally explored on living guinea pigs [Fattal *et al.* (1989)], in single living cells [van Manen and Otto (2007)] or in synthetic model systems [Discher *et al.* (1999)]. Synthetic membrane-enclosed structures are very similar to those occurring in biological system. Despite the differences in the chemical composition, both types of membrane show similar properties [Lomas *et al.* (2007)],[Battaglia and Ryan (2005)]. Furthermore synthetic membrane show a very good compatibility with tissue. Thus, they are a suitable tool for the above mentioned area of application.

A biological membrane is a thin sheet composed of two outer hydrophilic layers and an inner hydrophobic layer. This surface contains a large number of molecules composed which are comprised of two blocks, one is a polar phosphate group that is attracted to water and the other is apolar and repels polar molecules. This double nature of the two block gives rise to the name *amphiphile*. The apolar part is *hydrophobic* and is formed by one or two chains of repeating hydrocarbon units covalently bonded. The polar part is *hydrophilic* and tends to extend into the solvent due to the repulsive interaction with the bilayer's exterior

A lower energy configuration, in order to minimise the system free energy, the contact area of the apolar blocks with the solvent is reduced. In the optimal configuration the apolar blocks are completely shielded from the solvent by the polar block. A phospholipid molecule is characterise by a mean shape assigned by the size of the electronic clouds and the interaction with the solvent. The chains approach each others realising the best packing combination which is compatible with their shape [Israelachvili (1998)]. If the occupied volume of a amphiphile is a cone the chains will arrange in a spherical shape where all the tails go towards the centre. This structure is called *micelle*. If the chain is similar to a truncated cone the structure formed will have the shape of a worm. If the mean shape is cylindrical the chains arrange parallelly to each other with the same orientation. Two of these leaves face each other with opposite orientations and form a double layer denoted as a membrane. Large bilayer membranes bend and form a *vesicle*, where the membrane avoids free edges.

In the former description of the self assembled structures, we only mention the gross features of the molecular and the amphiphilic natures of the head and tail groups. This suggest that different chemical substances that have the same amphiphilic nature and have a similar mean shape will form similar structures. The degree of hydrophobicity of a substance can be defined by its characteristic *solubility* in a certain solvent. In amphiphilic polymers the hydrophobic and hydrophilic blocks are comprised of many identical repeating units, which are denoted monomers. The presence of oxygen or nitrogen in a monomer can cause an unequal sharing of the electrons and hence a good solubility in polar solvent, e.g. ethylene glycol, dodecanol acrylate. Other monomers exhibit an apolar nature, e.g. butadiene, isoprene, arkopal acrylate. These monomers can be connected via covalent bonds along the backbone of the chain molecule or

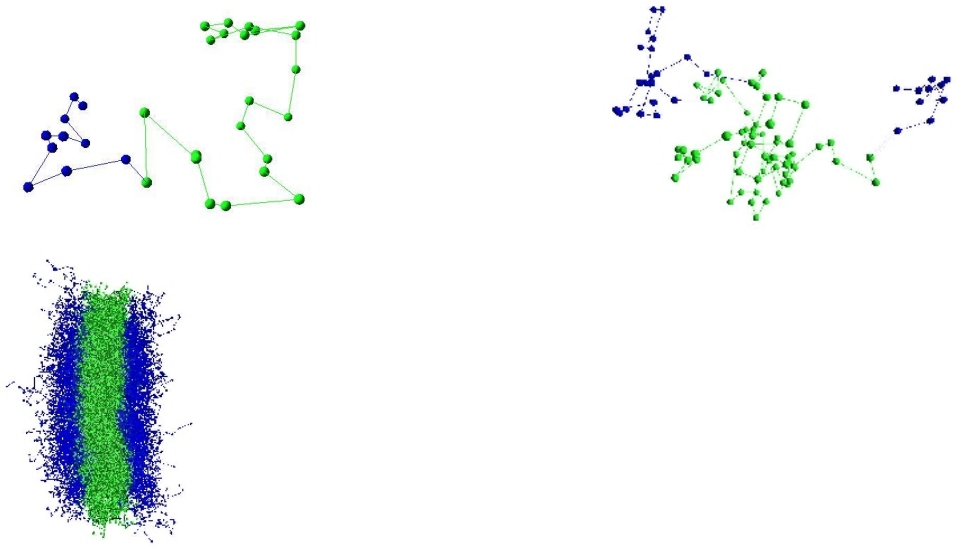

Figure 1: Simplistic visualisation of the structure of a chain. The green beads represent the hydrophobic tail group of the chain and the blue ones the hydrophilic head group. All the beads in a chain are connected by covalent bonds. The first picture from the left shows the structure of a single chain, the second three chains where the hydrophobic blocks are shielded by the hydrophilic blocks that face the solvent. The last picture on the right shows the positioning of all chains that form a membrane. In this side-view is it possible to see the separation between the inner layer and the outer ones.

polymer. An amphiphilic chain is composed of the schema $(X)_n - b - (Y)_m$ where X is apolar and Y is polar. The composition of the chain gives rise to different morphologies due to the particular mean shape of the polymer [Maskos (2006)]. These polymers can self-assembly into the previously quoted structures and this biological compatibility has attracted recent interest [Jin *et al.* (2007)], [Wang *et al.* (2007)]. Both synthetic polymeric vesicles, *polymersome*, and lipid vesicle, *liposome*, can be loaded with different polymers or antibodies that provide a compatibility with the target cells and carry the important drug or metals for medical or imaging purposes, [Torchilin (2005)].

The interest in polymersomes is supported by the recent ease to synthesise different architectures that self assemble into vesicles [Discher *et al.* (1999)], [Christian *et al.* (2008)]. Some important differences are to be noted between liposomes and the polymersomes. Polymeric amphiphiles have much higher molecular weights compared to phospholipids and can self-assemble into more entangled membrane improving mechanical properties to the final structure. Polar polymers like poly(2-(methacryloyloxy)ethyl phosphorylcholine), (PMPC) or poly (ethylene glycol), (PEG) , can be jointed to hydrophobic polymers with higher molecular mass and, in order to fabricate polymersomes which have a longer circulation time [Lasic (1994)]. The amphiphilic copolymers have a very low critical aggregation concentration (i.e. the minimal concentration necessary to form micellar aggregates). Moreover, the polymeric amphiphiles have a very slow chain exchange dynamics and hence a slow rate of dissociation allowing the retention of the payload for very long time periods.

Nanoparticles generally consist of a solid metallic or a semiconductor core surrounded by a shell of short polymer chains grafted onto the core. The presence of the polymer chains facilitate the dispersion in polymer melts. The size of the nanoparticle is ranged in the nano-meter scale $1 - 100[nm]$. The nanoparticles can easily diffuse into organic liquids and depending on the different coating they can bond to different tissues. The core of the nanoparticles, being metallic, can interact with external fields.

Gold cores are particularly interesting because of the high stability and biological compatibility and a variety of different coating are studied and produced [Krüger (2008)], [Jackson *et al.* (2004)], [Gentilini *et al.* (2008)]. In the case of gold nanoparticles the core can be produce to resonate to a certain wavelength and bind to malignant cells. Under the exposition of tuned infrared waves the gold nanoparticle heats up and kills the tumoral cells. The external field can also drive the nanoparticle into the cell via electroporation [Vuyst *et al.* (2008)]

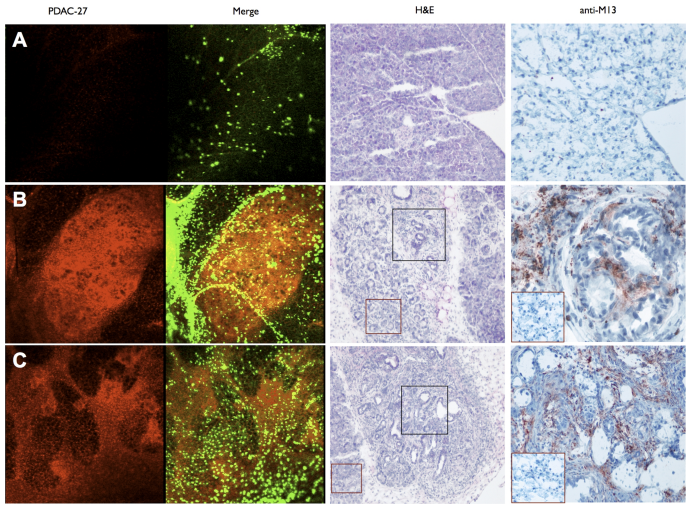

Figure 2: Visualisation of imaging capabilities of the nano-particle techniques. The images shows their localisation in a tumor. [Kelly *et al.* (2008)] ©Common Creatives Share Alike

In the case of semiconductor cores (e.g. ZnS, $CdSe$), that can be surrounded by an additional shell (zinc sulfide), the nanoparticles have a particular fluorescent emission that can trace the position of the cell to whom they are bonded [Kim *et al.* (2007)], [Kelly *et al.* (2008)] (Fig:). This new imaging technique will improve the knowledge of processes between the cells incorporating the nanoparticles. The nanoparticles are also used to deliver some important pharmacological drugs that would otherwise fail to reach the target or affect other tissues. The coating of a nanoparticle can change via external stimuli or different chemical composition of the surrounding fluid.

In the present work we want to study the stability of the inclusion of an apolar nanoparticle into the hydrophobic shell interior of a membrane. The stability is conditioned by the types of interaction and the size of the external entity. This research is performed by simulating a stable amphiphilic bilayer to which an external particle is added.

The large number of cooperating bodies involved in describing a membrane is really demanding. In the simulations runs a typical system consists in a thousand of chains and every chain is comprised of many beads. The molecular mass of molecule of water is eight hundreds times smaller than the polymers we simulated. A solvent molecule (water) is much smaller that that of an amphiphilic polymer. Since the dimension of the simulation box is in most of the case six or seven times larger than the thickness of the membrane and it would contain an excessive number of solvent molecules, a few millions, most of them non directly interacting with the chains. The universality illustrated in the previous argumentation suggests, however, to focus only on the relevant structural details. A common practice is to lump a group of interacting atoms or molecules into a single *bead* and reformulate the interactions in terms of effective interactions between the *mesoscopic* beads. The method is called *coarse graining* and it is widely used in simulating membranes [Müller *et al.* (2006)]. Further more, the elimination of the molecules of the solvent molecules significantly reduces

the number of interactions to be compute and the calculation can be restricted on the interactions between the amphiphiles.

The description of the nanoparticle in coarse-grained approach should also remove some structural details that are not essential on the mesoscopic scale. We propose to describe the nanoparticle via a potential that considers the hard core repulsion and an attractive short-ranged interaction with the hydrophobic beads of the amphiphiles.

In the second chapter we refer to a particular experimental set-up, [W.Müller *et al.* (2008)], where hydrophobic *nile red* and *quantum dots*, sizing from 3 to 9 $[nm]$, were incorporated into the shell of a polymeric membrane. The experimental observations can provide a confirmation of our simulation results. Is therefore important to configure the initial parameters to best mimic the referred system and to obtain from the simulation quantities that are experimentally measurable.

After the modelling of the system we proceed in the third chapter to study the stability of the nanoparticle in relation of its fundamental characteristics. In the last chapter we provide the condition for the stability and we briefly analyse the interplay of the different contributions.

The thesis ends with a discussion of the results obtained and a look-ahead at the possible scenarios that can be investigated by this model.

Chapter 1

Model and Theory

To describe the system, nanoparticle and membrane, we proceed via different steps. We want to create a model to simulate a homopolymer melt, stable in temperature and constant in density. Once the stability of the homopolymer is provided we add a new species and define the mutual interactions. The two types of beads are bonded together and form the two blocks for the amphiphilic molecule. These amphiphiles self-assemble into bilayer membranes. The interaction between the two species is proportional to the *incompatibility* between the two species. This parameter characterises a typical distributions of the amphiphilic molecules and the thickness of the hydrophilic part. Once the equilibrium properties of the membrane is modeled setting the appropriate boundary conditions, a nano particle can be added in the middle of the two leave of which the bilayer is composed.

To characterise the homopolymer melt we use, as mentioned in the introduction, a coarse-grained description in a solvent-free model. The forces that rule the dynamics are not longer interatomic or intermolecular interactions, as explained in [Israelachvili (1998)], but derive from an effective Hamiltonian that comprises all the interaction with the solvent molecules, which have been integrated out, and the mesoscopic beads. Due to the pronounced hydrophobicity of the hydrocarbon chains in the solvent (water) we assume that the homopolymer melt is phase separated from the solvent. In a solvent-free model we have a coexistence between a liquid phase, the melt, and a vacuum phase, the solvent. The effective Hamiltonian is defined by a third-order virial expansion, i.e. the lowest-order approximation for a separation of a separation between a liquid and a vapour phase. From the effective Hamiltonian we can derive the forces that rule the dynamics and the equation of state of the system. The melt of hydrophobic chains forms an almost incompressible system with a specific density ρ_0.

The hydrophilic beads are in good solvent condition and a second-order equation of state suffices to define their interactions. To describe the amphiphiles we create a chain separated in two blocks, one composed by hydrophobic beads and the other by hydrophilic. The effective Hamiltonian includes the interactions between the two different types of bead. Once the interactions are defined we arrange the amphiphiles in a bilayer and run a simulation to verify that the system is stable in temperature and the bilayer do not rupture.

A coarse-grained description should be invariant under changing the discretisation, i.e. a different choice of number of beads per chain molecule, N_b, should define the same physical system. The parameters that quantify the strength of the interactions are hence redefined to be non-dimensional and independent of the discretisation.

The calculation of the dynamics is performed by multibody dissipative particle dynamics, (MDPD), a simulation scheme that uses a weighting function, which renders the interactions soft. The softness of the forces permits to increase the time step of the simulation without alter the stability of the algorithm. Being a mesoscopic simulation the calculation of the forces should include a dissipative and random contribution due to the Brownian noise of the microscopic particles (solvent), whose degree of freedom have been integrated out. The strength of these contributions is set by the dissipation-fluctuation theorem that guarantees a reliable thermostatting. The

experimental systems are often in contact with a thermal reservoir and kept at a fixed temperature. One of the most important characteristics of thermostat in the MDPD method is the local conservation of the momentum. The integration of the equation of motion is led by the velocity Verlet algorithm. The properties of the simulation scheme are briefly introduce in the following sections.

Once the membrane is created we introduce a description of the nanoparticle that interacts with both types of beads: it is repulsive towards the hydrophilic beads and attracts the hydrophobic, save for the hard core repulsion. Even the nanoparticle has thermostatting forces, whose strengths, depends on the radius of the nanoparticle.

1.1 Solvent-Free Model

Equation of state

An equation of state can be formulated as a *virial* expansion in powers of density where every virial coefficient represents a n-body interaction.

$$P = k_B T \sum_{n=1} c_n \rho^n \tag{1.1}$$

The first order term, $c_1 = 1$ represents an ideal gas where no interaction occurs between the particle. Further terms are required when pairwise interactions, $c_2 \neq 0$, or multi-body interactions, $c_{n>2} \neq 0$, occur. Homopolymer chains in a polar solvent aggregates each other and form a *melt* that minimise the unfavourable contacts with the solvent. The system is nearly incompressible and the melt locally conserves the same density. Since we have removed the solvent the pressure of the whole system is zero because the polymer melt coexists with a vapour of vanishingly low density (basically vacuum) and at the equilibrium the pressure must be the same in every point of the space. The equation of state, $P(\rho)$, that describes the coexistence of the homopolymer melt in a fluid phase with its vapour is at the lowest order a third degree polynomial, i.e. the lowest order curve that cross the point $(0, 0)$ and $(0, \rho_{coex})$. The phase line has a physical meaning only on the upper side of the diagram for positive pressure. For densities that correspond to negative pressures (miscibility gap), phase separation occurs and the system is spatially inhomogeneous. In the graph, (Fig: 1.1), we show

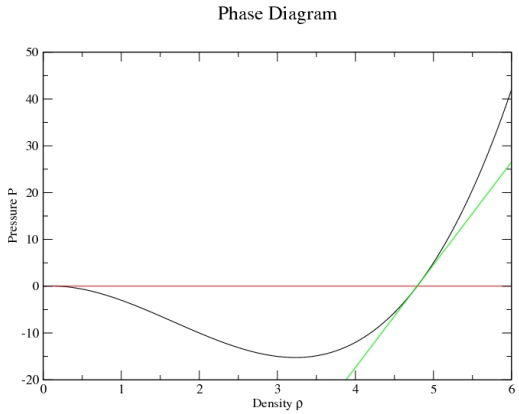

Figure 1.1: Mean-field Equation of state of the liquid-vapour interface. The curve represent the third-order polynomial expansion of the equation of state, the tangent shows the derivative of the equation of state with respect to the density, i.e. the reciprocal of the compressibility of the system

the line represented by the equation

$$\frac{P}{k_B T} = \rho + c_2\rho^2 + c_3\rho^3 \tag{1.2}$$

in which the density of coexistence is represented in the point where the line crosses the abscissa. The straight line shown in the graph marks the inverse of the compressibility of the system. Usually the incompressibility of the system adopts a small value, on the mesoscale, the system is considered as incompressible, and the density has an upper limiting density $0 < \rho(r) < \rho_0$. The coexistence density of the hydrophobic melt and the thickness of the bilayer membrane in the tensionless state dictate the areal density of amphiphiles in a bilayer membrane. This is a key characteristics of the membrane and values for different system are available int the literature [Bermudez *et al.* (2002)],[Bermudez *et al.* (2004)] the values range around $\rho_c = 10 - 100[R_e^{-3}]$ in units of R_e, end-to-end distance of the chain.

Implicit Solvent

The number of molecules of the surrounding solvent is predominant and if it were included explicitly, it would demand most of the computational time during a simulation. Most of these molecules do not interact directly with the membranes. A common practice to reduce the calculation time is to integrate out the solvent degrees of freedom. The interactions between the monomers are hence described by an effective Hamiltonian. This approach comprises all the interactions between the particles to build a potential whose derivative furnishes an average force that, statistically, represents the hidden interaction with the "ghost" solvent molecules.

There is another important motivation to remove the molecules of the solvent. Recalling the Gibbs phase rule

$$f = 2 + c - \phi \tag{1.3}$$

we can establish how many independent intensive variables f are necessary to describe c number of components of ϕ number of phases in an interface. Since we have removed the molecules of the solvent only the amphiphilic chains remain, $c = 1$, in a one-phase state, $\phi = 1$. The number of intensive thermodynamical variables necessary to describe our system are two, $f = 2$. We can express two intensive variables in the canonical ensemble NVT, or in an ensemble where the tangential pressure is constant, NP_tT, that will be useful in our simulation.

The effective Hamiltonian of the system is described as a functional of the density. We can obtain the equation of state previously defined writing the Hamiltonian as an expansion up to the third order in density. The functional formulation of this potential is

$$\frac{H[\rho]}{k_B T} = \sum_{\alpha,\beta,\gamma\in\{A,B\}} \int \frac{\mathrm{d}^3 r}{R_e^3}\Big(\frac{v^2_{\alpha\beta}}{2}\rho_\alpha\rho_\beta + \frac{v^3_{\alpha\beta\gamma}}{3}\rho_\alpha\rho_\beta\rho_\gamma\Big) \tag{1.4}$$

where the greek indices specify the type of the species.

We can see how this Hamiltonian leads us to the same equation of state. The pressure is obtainable as the partial derivative of the free-energy respect to the volume.

$$P = -\frac{\partial}{\partial V}F = k_B T\frac{\partial}{\partial V}\ln Z \qquad Z = \int e^{-\beta H(r)}\mathrm{d}^3 r^N \tag{1.5}$$

Since the potential does not depend on the direction we perform the following substitution

$$\boldsymbol{r} = V^{1/3}\boldsymbol{r}' \tag{1.6}$$

The scaled positions $\boldsymbol{r}'$ have the interesting property that the scale coordinates of all the particles remain fixed even if we expand or contract the system. Substituting we obtain

$$P \;=\; k_B T\partial_V \ln\Big(V^N\int \mathrm{d}\boldsymbol{r}'^N e^{-\beta H(V^{1/3}\boldsymbol{r}')}\Big) = \frac{k_B T N}{V} - \langle\partial_V H(V^{1/3}\boldsymbol{r}')\rangle \tag{1.7}$$

The total force that acts on a single particle is $\boldsymbol{F}_i^{tot} = -\nabla_{\boldsymbol{r}_i} H(r)$. We can hence rewrite the last term of the previous equation as

$$-\langle \partial_V H \rangle = -\frac{\langle V \partial_V H \rangle}{V} = -\frac{\langle \sum_i^N \boldsymbol{r}_i \nabla_i H \rangle}{V} = \frac{\langle \boldsymbol{r}_i \boldsymbol{f}_i^{tot} \rangle}{V} =: \frac{W}{V} \tag{1.8}$$

where the we have introduce the virial W. In the previous calculation we utilise the equivalence of ensemble is that the basic thermodynamics properties may be calculated as averages in any convenient ensemble [Allen and Tildesley (1991)]. If we consider only one species $\alpha = \beta = \gamma = A$ for the Hamiltonian (1.4) the virial is

$$W = V\langle \partial_V \int \mathrm{d}^3 r' \Big(\rho_A^2 \frac{v_A A}{2} + \rho_0^3 \frac{2 v_{AAA}}{3} \Big) \rangle = V \Big(\frac{v_{AA}}{2} \rho_0^2 + \frac{2 v_{AAA}}{3} \rho_0^3 \Big) \tag{1.9}$$

yielding to a third-order equation of state.

A molecular dynamics simulation integrates the equation of motion of a system of particles. We must hence provide a description of forces acting between a certain number of particles. The density functional formulation of the Hamiltonian of interaction in (1.4) in terms of the local density, ρ, provides a definition of the forces that act between the particles. In our model, a polymer chain is described by a bead-spring model with two different types of beads that we mark A for the hydrophobic bead and B for the hydrophilic. Neighbouring beads along the backbone of the chain molecule are connected by harmonic spring. In our model described the conservative interactions, F^c, are the sum of bonded, b, and non-bonded, nb, forces.

$$\boldsymbol{F}^c = \boldsymbol{F}^{nb} + \boldsymbol{F}^b \tag{1.10}$$

The the strength of the forces acting on the beads depends on the particular discretisation used.

Discretisation

The Hamiltonian of the system is an invariant with respect to changing the discretisation and the length scale of the system. This means that we have to define the virial coefficients with respect to the length scale, R_e, and to discretisation, N, used.

The length scale, R_e, denotes the mean-square end-to-end distance of the polymer. For a freely-jointed model one obtains:

$$\langle R_e^2 \rangle = \sum_{ij} \langle \boldsymbol{r}_i \boldsymbol{r}_j \rangle = l^2 \sum_{ij} \langle \cos\theta_{ij} \rangle = l^2 \sum_{ij} \delta_{ij} = l^2 n \tag{1.11}$$

using $\langle \cos\theta_{i \neq j} \rangle = 0$. l is the statistical length. Its value depends on the chemical structure of the monomers and it is known and tabulated for a variety of different polymer material [Mark (2007)]. The volume and the density of the system are rescaled in units of the end-to-end distance, R_e, and the number of beads per chain, N_b

$$V \mapsto \frac{V}{{R_e}^3} \qquad \rho \mapsto \rho \frac{{R_e}^3}{N_b} \tag{1.12}$$

This imply that the virial coefficients depend on the end-to-end distance and on the discretisation to preserve the invariance of the Hamiltonian.

$$\begin{aligned} \frac{H}{k_B T} &= \int \frac{\mathrm{d}^3 r}{{R_e}^3} \Big(\frac{v_2'}{2} \rho'^2 + \frac{v_3'}{3} \rho'^3 \Big) = \\ &= \int \mathrm{d}^3 r \Big(\frac{v_2' R_e^3}{2 N_b} \frac{\rho'^2 N_b^2}{R_e^6} + \frac{v_3' R_e^6}{3} \frac{\rho'^3 N_b^3}{R_e^9} \Big) = \int \mathrm{d}^3 r \Big(\frac{v_2}{2} \rho^2 + \frac{v_3}{3} \rho^3 \Big) \end{aligned} \tag{1.13}$$

i.e. the virial coefficients and the density scale with the following relations

$$\rho \mapsto \frac{\rho R_e^3}{N_b} \qquad v_{\alpha\beta} \mapsto \frac{v_{\alpha\beta} N_b^2}{R_e^3} \qquad v_{\alpha\beta\gamma} \mapsto \frac{v_{\alpha\beta\gamma} N_b^3}{R_e^6} \tag{1.14}$$

Also the bonded interactions depend on the discretisation. For computational simplicity, we do not utilise a freely jointed chain model with a fixed bond length but successive monomers are bonded by a harmonic potential. This is the minimal model that gives rise to Gaussian statistics of the chain conformations. The bonded interactions are given by a discredited Edwards-Hamiltonian:

$$\frac{H_b[\boldsymbol{r}_s]}{k_BT} = \sum_{i=1}^{N_b-1} \frac{3(N_b-1)}{2R_e^2}(\boldsymbol{r}_i - \boldsymbol{r}_{i+1})^2 \tag{1.15}$$

Virial Coefficients

The Hamiltonian of non-bonded interaction considers interactions between beads of the same species, $A-A$, $B-B$, and cross interactions $A-B$. We must hence estimate seven virial coefficient: v_{AA}, v_{AB}, v_{BB}, v_{AAA}, v_{BBB}, w_{ABB} and w_{AAB}. The virial coefficients characterise the different interactions between the species of beads and parametrise the equation of state. The hydrophilic head groups are in good solvent condition. A polymer in good solvent condition can be represented by a chain in which only the two-body interaction are relevant and hence, $v_{BB} > 0$ and $v_{BBB} = 0$, [Fredrickson *et al.* (2002)]. For the hydrophobic tails higher orders are to be take into account. We consider polymer melt compose by hydrophobic chains. The first coefficient represent the ideal gas and is equal to one $v_A = 1$. An equation of state up to the third order, which is capable of describing the coexistence between a dense hydrophobic melt and its vapour, requires that the second order term is negative, $v_{AA} < 0$, and the third is positive, $v_{AAA} > 0$. The second- and third-order coefficients can be determined from the following reasoning: a first equation is provided by the fact that in an implicit solvent the external pressure at the coexistence vanishes and the melt in equilibrium has the same pressure

$$P \simeq 0 \simeq \rho_0 + \frac{v_{AA}}{2}\rho_0^2 + \frac{2v_{AAA}}{3}\rho_0^3 \tag{1.16}$$

A second equation is obtained from the isothermal incompressibility defined by

$$\frac{1}{k_T} = -V\Big(\frac{\partial P}{\partial V}\Big)_T = \rho_0\partial_\rho\Big(\rho + \frac{v_{AA}}{2}\rho^2 + \frac{v_{AAA}}{3}\rho^3\Big) = \rho_0 + v_{AA}\rho_A^2 + v_{AAA}\rho_0^3 \tag{1.17}$$

For a homopolymer melt, the thermal compressibility is given by

$$\frac{1}{k_T} = \rho_0\partial_\rho P = \rho_0\partial_\rho(k_BT\rho + \langle\partial_\rho H_I(\rho)\rangle) = \rho_0 k_BT(1 + \partial_\rho W) \tag{1.18}$$

where we recall the definition of the virial in eq. 1.8. We call κ the derivative of the virial with respect to the pressure $\kappa := \partial_\rho W$, where the thermal incompressibility is also defined in terms of the Edwards correlation length, ξ [Wu *et al.* (1995)]

$$\frac{\beta}{k_T} = \frac{\rho_0}{12(\xi/R_e)^2} \tag{1.19}$$

where β is the Boltzmann factor, $\beta = (k_BT)^{-1}$. The characteristic length in the solution is the Edwards correlation length which is connected to the statistical segment length of an ideal chain, b, and the excluded volume, v, (positive in good solvent condition) [Meyer *et al.* (2008)].

$$\xi = \frac{b}{(12\rho v)^2} \tag{1.20}$$

The mixed terms can be calculated in using a theory of miscibility between two different species. The entropy favours the miscibility of the two components but the repulsive forces tend to separate them. The Flory interaction parameter, χ, characterises the difference of interaction energies in the mixture. The theory considers a blend of two different components, the component A and the component B which are chemically

different. The component A occupies the volume V_A and ϕ_A is the volume fraction of the A species, $\phi_A := V_A/V_{tot}$. The free energy of mixing, ΔG_m, is the change in energy when two different chemical substances are mixed. The free energy of mixing for pure components, considered separated, is the sum of an entropic, ΔS, and an enthalpic term, ΔH. Is the volume is totally occupied by the two species $\phi_a = \phi$ and $\phi_b = 1 - \phi$

$$\frac{\Delta G_m}{RT} = \Delta H_m - T\Delta S = \frac{\phi}{N_A}\ln\phi_A + \frac{(1-\phi)}{N_B}\ln\phi_B + \phi(1-\phi)\chi \tag{1.21}$$

The Flory-Huggins equation, on the right hand side, is the sum of combinatorial and interactional terms where R is the gas constant. Following [Müller (1999)] we can define the χ parameter calculating the difference of the chemical potential per monomer between the two species. Neglecting fluctuations we can define χ as:

$$\chi = \rho \int \mathrm{d}^3 r \Big(g_{AB}(\boldsymbol{r}) U_{AB}(\boldsymbol{r}) - \frac{g_{AA}(\boldsymbol{r})U_{AA}(\boldsymbol{r}) + g_{BB}U_{BB}(\boldsymbol{r})}{2} \Big) \tag{1.22}$$

where $g_{\alpha\beta}$, with $\alpha, \beta \in \{A, B\}$, is the pair correlation function between the monomer of the species α with the monomers with the species β and $U_{\alpha\beta}$ is the pair-wise potential energy between the two species. In a mean-field approximation the pair correlation function is $g(\boldsymbol{r}) = 1$ and the integration of the potential yields to the second-order virial coefficients.

$$\begin{aligned} \chi &\simeq \frac{\rho}{K_B T} \int \mathrm{d}^3 r \Big(U_{AB}(\boldsymbol{r}) - \frac{1}{2}\big(U_{AA}(\boldsymbol{r}) + U_{BB}(\boldsymbol{r})\big) \Big) = \\ &= \rho \Big(v_{AB} - \frac{1}{2}\big(v_{AA} + v_{BB}\big) \Big) \end{aligned} \tag{1.23}$$

In the Helfand's model, [Helfand and Tagami (1971)], the previous theory is extended for a nearly incompressible system $\phi_A + \phi_b \lessapprox 1$

$$\frac{H_I}{k_B T} = \chi\rho_0 \int \mathrm{d}^3 r \mathrm{d}^3 r' \phi_A(r)\phi_B(r) + \frac{\kappa}{2}\rho_0 \int \mathrm{d}\boldsymbol{r} (\phi_A(r) + \phi_B(r) - 1)^2 \tag{1.24}$$

where the κ parameter express the tendency of the system to pull the polymers into regions where the total density is $\rho_A + \rho_B = \rho_0$.

The density of the system, ρ_0, depends on the number of beads per chain, N_b. If we change the discretisation the number density of beads in the system will change. Since $\rho_0\kappa$ and $\rho_0\chi$ are invariant, if we refer in units of the chain density $\rho_c = \rho_0/N_b$, κN and χN are invariant. Combining (1.16), (1.17) and (1.23) we obtain the virial coefficients

$$\begin{aligned} v_{AA} = -2\frac{\kappa N + 3}{\rho_0} \qquad v_{AAA} = \frac{3}{2}\frac{\kappa N + 2}{\rho_0^2} \\ v_{AB} = \frac{\chi N}{\rho_0} + \frac{1}{2}(v_{AA} + v_{BB}) \end{aligned} \tag{1.25}$$

The evaluation of the other parameters is empirical. The remaining two third order mixed terms v_{ABB}, v_{AAB} should be positive and for simplicity we equal them to the v_{AAA} term: $v_{AAA} = v_{AAB} = v_{ABB}$. Choosing $v_{BB} = 0.1$ provides a bilayer stability while larger values contribute to create micelles instead of bilayers.

1.2 Dissipative Particle Dynamics

To simulate the dynamics of the polymers or lipids in the membrane we use the DPD (Dissipative Particle Dynamics) simulation method. The original work from [Koeleman and Hoogerbrugge (1993)] was successive upgraded by [Pagonabarraga and Frenkel (2001)] into a MDPD (Multi body Dissipative Particle Dynamics) scheme which we explain below.

DPD Dissipative Particle Dynamics

MDPD Multi body Dissipative Particle Dynamics

DPD is a method to integrate the equation of motion like molecular dynamics simulation but its range of validity is the mesoscopic scale and therefore requires a Brownian noise that could include the hidden interaction with the "ghost" microscopic particle. In contrast to a Langevin description, DPD uses a noise and friction that locally conserves angular and linear momentum. The conservation of the hydrodynamics is important in annealing defects [G.Gonnella *et al.* (1997)]. For the DPD thermostat the equation of motion is the sum of conservative (c), dissipative (d) and random (r) forces

$$m\dot{\boldsymbol{v}} = \boldsymbol{F}^c + \boldsymbol{F}^d + \boldsymbol{F}^r \tag{1.26}$$

$\boldsymbol{F}^c$ conservative
$\boldsymbol{F}^d$ dissipative
$\boldsymbol{F}^r$ random

Every component is limited within a range interval, r_c, by a weighting function $w(r_{ij})$ that depends on the relative distance between the particles. This function is 1 for $r = 0$ and goes to zero at the cut-off distance $r = r_c$. Every force is pair-wise and conserves locally momentum.

$$m\dot{\boldsymbol{v}} = w^c(r_{ij})\boldsymbol{f}^c_{ij} + w^d(r_{ij})\boldsymbol{f}^d_{ij} + w^r(r_{ij})\boldsymbol{f}^r_{ij} \tag{1.27}$$

$\boldsymbol{f}_{ij}$ strength of the force acting between the i and j particle

The weighting function makes the forces soft and permits to increase the time-step of the simulated system [Pastorino *et al.* (2007)].

The conservative force depends on the particular system and it is obtained from the derivative of the potential. The dissipative and random forces should obey the dissipation-fluctuation theorem. If we determine a dissipative term γ we have to define the strength, ξ. As shown in [Orlandini (2008)] if we choose an uncorrelated Gaussian random noise (we suppose that the system relaxation time is shorter than the time step) with zero average

$\gamma(\boldsymbol{v}_{ij}\hat{\boldsymbol{r}_{ij}})\hat{\boldsymbol{r}}_{ij} := \boldsymbol{f}^d_{ij}$

$$\langle\theta^g_{ij}(t)\rangle = 0 \qquad \langle\theta^g_{ij}(t)\theta^g_{kl}(t')\rangle = (\delta_{ik}\delta_{jl} + \delta_{il}\delta_{jk})\delta(t - t') \tag{1.28}$$

the strength terms should satisfy the relation

$$\xi = \sqrt{2\frac{\gamma k_B T}{m\Delta t}} \tag{1.29}$$

In practise, following [Dünweg and Paul (1991)], we can use a uniform random number generator, θ^u_{ij}, which is faster to compute, instead of a Gaussian. In that case we should consider that if a Gaussian distribution has a variance of σ, a uniform distribution equal to 1 between $[-\sigma/2, \sigma/2]$ has a variance $\sqrt{12}\sigma$. Hence, our equation of motion takes the form

$$m\dot{\boldsymbol{v}} = \boldsymbol{f}^c_{ij}w^c(r_{ij}) - \gamma w^d(r_{ij})(\boldsymbol{v}_{ij}\hat{\boldsymbol{r}}_{ij})\hat{\boldsymbol{r}} + \sqrt{\frac{24\gamma k_B T}{m\Delta t}}\theta^u_{ij}w^r(r_{ij}) \tag{1.30}$$

In Groot and Warren's work [Groot and Warren (1997)] the DPD simulation method is widely investigate and following their results, we set $\gamma = 0.1$ and $\Delta t = 0.01$ in the system's units: $k_B T = r_c = m = 1$. From the suggestions of the same work we use the velocity Verlet integration scheme instead of the Euler's. Español and Warren (1995) [Espanol and Warren (1995)] have shown that the dissipative weighting function can be chosen arbitrary and is connected to the random weighting function by the relation $w^d(r) = (w^r(r))^2$. In [Pastorino *et al.* (2007)] different weighting functions in different polymer system are tested. The particular choice of a weighting function concerns the thermostat of the system and the computational efficiency. We define the number of particles thermostated, i.e. the particle include in the sphere within the cut-off multiplied by the weighting function, as

$$N_{TP} = \rho_0 \int_0^r w^r(r)g(r)4\pi r^2 \mathrm{d}r \tag{1.31}$$

where the $g(r)$ in the pair correlation function that in our case we approximate 1. The use of the following weighting function

$$w^d(r) = (w^r(r))^2 = \left(1 - \frac{r}{r_c}\right)^2 \quad \text{if} \quad r < r_c \tag{1.32}$$

provides a fast computing efficiency. In agreement with the suggestions of [Hömberg (2008)] and [Trominov *et al.* (2002)], we observe in our simulations that if the cut-off distance include an average number of thermostated particle larger than 3-4 the system conserves temperature keeping a time step of $\Delta t = 0.01$.

The integration of the equations of motion is performed via a velocity Verlet algorithm which is composed in two steps

$$\boldsymbol{r}_i(\Delta t) = \boldsymbol{r}_i(0) + \Delta t \dot{\boldsymbol{r}}_i(0) + \frac{\Delta t^2}{2m_i}\boldsymbol{F}_i(0) \qquad \dot{\boldsymbol{r}}_i(\Delta t/2) = \dot{\boldsymbol{r}}_i(0) + \frac{\Delta t}{2m_i}\boldsymbol{F}_i(0)$$

and secondly

$$\dot{\boldsymbol{r}}_i(\Delta t) = \dot{\boldsymbol{r}}_i(\Delta t/2) + \frac{\Delta t}{2m_i}\boldsymbol{F}_i(\Delta t) \tag{1.33}$$

and its derivation is briefly discussed in the appendix.

Conservative Force

The non-bonded interactions between the beads should come from the negative derivative of the potential.

$$\boldsymbol{F}_{\alpha\beta}(r_i, r_j) = -\nabla_{\boldsymbol{r}} U(r_\alpha, r_\beta) \tag{1.34}$$

where the Greek indices refer to the different types of beads, A, B. The forces depend on the type of beads involved and on the mutual distance. It is now important to show how we obtain a pairwise interaction which is required from the DPD simulation scheme. The Hamiltonian we use for a one component system is, $v_2 := v_{\alpha\alpha}$, $v_3 := v_{\alpha\alpha\alpha}$

$v_2 := v_{\alpha\beta}$
$v_3 := v_{\alpha\beta\gamma}$

$$\frac{H}{k_B T} = \int \mathrm{d}^3 r \Big(\frac{v_2}{2}\rho^2(\boldsymbol{r}) + \frac{v_3}{3}\rho^3(\boldsymbol{r}) \Big) \tag{1.35}$$

If we consider our particles as points we write the density as a sum of delta functions

$$\rho(\boldsymbol{r}) = \sum_i \delta(\boldsymbol{r} - \boldsymbol{r}_i) \tag{1.36}$$

but since the product of delta functions is not defined we rewrite the product of density functions as a delta times a weighting function $\mathfrak{w}(r)$ to determine

$$\rho^2(\boldsymbol{r}) := \sum_{ij} \delta(\boldsymbol{r}_i - \boldsymbol{r}) \mathfrak{w}(|\boldsymbol{r} - \boldsymbol{r}_j|) \tag{1.37}$$

$$\rho^3(r) =: \sum_{ijk} \delta(\boldsymbol{r}_i - \boldsymbol{r}) \mathfrak{w}(|\boldsymbol{r} - \boldsymbol{r}_j) \mathfrak{w}(|\boldsymbol{r} - \boldsymbol{r}_k|) \tag{1.38}$$

This weighting function should be normalised

$$4\pi \int_0^{r_c} r^2 \mathrm{d}r \mathfrak{w}(r) = 1 \tag{1.39}$$

and will help us to formulate the Hamiltonian as a sum all over the positions of the particle, $r_{ij} := |\boldsymbol{r}_i - \boldsymbol{r}_j|$

$r_{ij} = |\boldsymbol{r}_i - \boldsymbol{r}_j|$

$$\begin{aligned} \frac{H_{nb}}{k_B T} &= \int \mathrm{d}^3 r \sum_{ij} \delta(\boldsymbol{r} - \boldsymbol{r}_i) \Big(\frac{v_2}{2}\mathfrak{w}(|\boldsymbol{r} - \boldsymbol{r}_j|) + \frac{v_3}{3}\mathfrak{w}(|\boldsymbol{r} - \boldsymbol{r}_j|) \sum_k \mathfrak{w}(|\boldsymbol{r} - \boldsymbol{r}_k|) \Big) \\ &= \sum_{ij} \Big(\frac{v_2}{2}\mathfrak{w}(r_{ij}) + \frac{v_3}{3}\mathfrak{w}(r_{ij}) \sum_k \mathfrak{w}(r_{ik}) \Big) \end{aligned} \tag{1.40}$$

The weighting function, $\mathfrak{w}(r)$, represents the coarse-graining operation, which implies that we cannot resolve the system below a certain length scale r_c. We finally obtain the conservative force deriving the potential respect to the coordinate $\boldsymbol{r}_i$

$\sum_j (\partial_i \sum_k \mathfrak{w}_{ik}) \mathfrak{w}_{ij} =$
$=$

$$\begin{aligned}
\boldsymbol{F}_i^{nb} &:= -\partial_{\boldsymbol{r}_i} H_{nb} \\
= - \; k_B T & \sum_j \Big(\frac{v_2}{2} \partial_{\boldsymbol{r}_i} \mathfrak{w}(r_{ij}) + \frac{v_3}{3} (\partial_{\boldsymbol{r}_i} \mathfrak{w}(r_{ij})) \sum_k \mathfrak{w}(r_{ik}) + \frac{v_3}{3} \mathfrak{w}(r_{ij}) \partial_{\boldsymbol{r}_i} r \sum_k \mathfrak{w}(r_{ik}) \Big) \\
&= -k_B T \sum_j \Big(\Big(\frac{v_2}{2} + \frac{2}{3} v_3 \sum_k \mathfrak{w}(r_{ik}) \Big) \mathfrak{w}'(r_{ij}) \hat{\boldsymbol{r}_{ij}} \Big) \\
&= \sum_j \boldsymbol{F}_{ij} \qquad (1.41)
\end{aligned}$$

Where we have used

$$\sum_j (\partial_i \sum_k \mathfrak{w}_{ik}) \mathfrak{w}_{ij} = \sum_j \sum_k (\partial_i \mathfrak{w}_{ik}) \mathfrak{w}_{ij} = \sum_j (\partial_i \mathfrak{w}_{ij}) \sum_k \mathfrak{w}_{ik}$$

In this way we have obtained a conservative pairwise force in agreement with the requirement of the MDPD simulation method.

1.3 Homopolymer Melt

As we have seen in the previous calculation the weighting function should be differentiable, without singularities and fast to compute. From (1.41) we can see that the definition of the weighting function changes the interactions. The definition of the weighting function is connected with the pair-correlation function and the effective potential.

The Boltzmann factor between two particles is $exp(-\beta U(r_{ij}))$ that reduce to 1 if the particles do not interact. The difference between the Boltzmann factor of the interacting and non interacting particle is defined as the Mayer function.

$$f(r) := e^{-\beta U(r)} - 1 \qquad (1.42)$$

that is a positive function for the attractive potential ($U(r)$ negative), negative for repulsive potential and zero for no interaction. The minus sign of the integral of the Mayer function quantify the excluded volume.

$$V_{ex} := \int \mathrm{d}^3 r \Big(1 - e^{-\beta U(r)} \Big) \qquad (1.43)$$

Choosing the Weighting Function

The weighting function is a function that goes to zero at the cut of distance and define the shape of the interaction around a bead and hence the mean shape described in the introduction. This shape influence the properties of packing of the anphiphilic chains a should change depending on the type of interaction. The choice of the weighting function is constrained to a computational efficiency. The faster curves to compute that are constant within $[0, a]$ and go to zero at the cut-off distance r_c with no singularities in its derivative are the splines. The setting of the order of the spline and the limit of the a value should represent the expected interaction.

For example, two different parameter, $a = 0.9$ and $a = 0.5$, of the weighting functions, [Hömberg (2008)] (1.44), changes the variation in the density at the liquid vapour interface.

$$\mathfrak{w}(r) = \begin{cases} \frac{2r^3 - 3(a+1)x^2 + 6ax - 3a^2 + 1}{(1-a)^3} & \text{if} \quad a < r < 1 \\ 0 & \text{if} \quad 1 < r < a \end{cases} \qquad (1.44)$$

The changing in the density profile respect to the a parameter can be explained in a heuristic way. If the a parameter is large the beads resemble like hard spheres. The narrow liquid-vapour interface acts like a hard wall and gives rise to pronounced packing. If we make the hard core of the spheres more soft, decreasing a, the beads

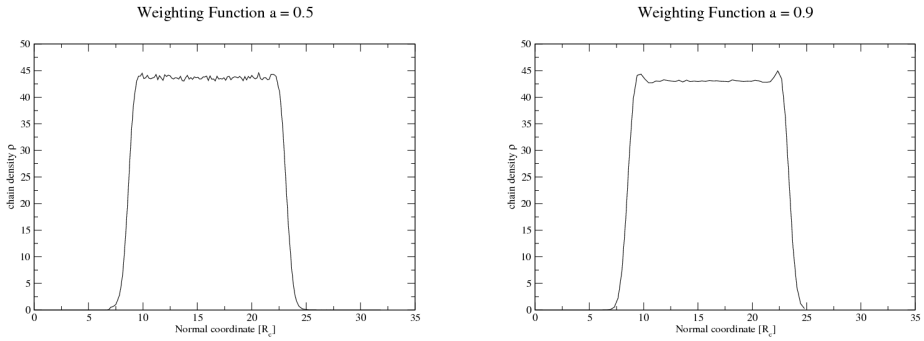

Figure 1.2: The change of the a parameter in the weighting function, from $a = 0.9$ to a $a = 0.5$ decreases density oscillation in the profile of the liquid vapour interface between a melt and vacuum.

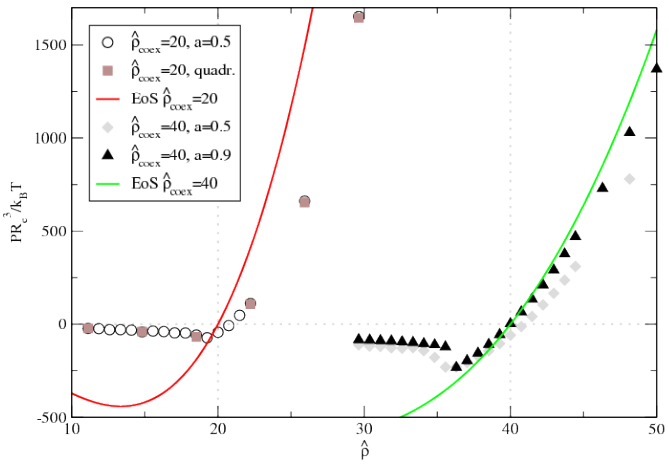

Figure 1.3: Comparison between the mean field equation of state using two different values of the parameter a of the weighting function. The best agreement is obtained in the case of a $\rho_{coex} = 40$ and $a = 0.9$. The agreement for a $a = 0.5$ is limited to small pressure. Courtesy M. Hömberg

more represent a soft particle volume than hard sphere and the packing is no longer observed.

In (Fig: 1.3), we observe that a large values, $a = 9$, yields better agreement between the pressure extracted from the simulations and the mean-field equation of state. Since we are interested in low densities, however, we choose $a = 0.5$ in the following.

1.4 Stable Bilayer

To simulate bilayers and study their stability we pre-assemble the amphiphilic molecules into a planar bilayer. The segment between the last A bead and the first B bead is disposed in two different parallel plane distant d_t. From the first position the hydrophilic beads are placed within the two planes one after the other using a Gaussian number generator. The hydrophilic blocks are placed in the same way outwards. Depending on

the input parameters the membrane realise a configuration homogeneous and stable in temperature for a determined thickness, d_t, and a ratio of chains per area R_{cpa}. The determination of this two parameters is discussed the next chapter where we discuss the mapping between simulated and real system.

1.5 Modelling the Nanoparticle

In the introduction we have presented a large class of nanoparticles. The nanoparticles can have different shapes and chemical compositions but, applying the same argument for the bilayer membrane we define a nanoparticle through its most important characteristics: the hard-core repulsion and the degree of hydrophobicity. The coarse-grained model do not resolve within a spatial length r_c, which is defined with the weighting function, and all the details below this length scale are unimportant. In the next chapter we discuss a comparison from the quantities used in our simulations to the experimental quantities and now we present a brief discussion on the inclusion of a nanoparticle in our model scheme.

Interaction

The interaction of the nanoparticle with the surrounding beads is provided by hard-core repulsion and a hydrophobic attraction. Therefore the interaction should be repulsive within the radius of the particle, $[0, r_{hc}]$, attractive only with the hydrophobic beads within a cut-off distance, $[r_{hc}, r_c]$, being the apolar interaction short ranged. A obvious choice is a Lennard Jones potential of the form

$$U(r) := h\Big(\Big(\frac{r_{hc}}{r}\Big)^9 - \Big(\frac{r_{hc}}{r}\Big)^3\Big) \tag{1.45}$$

which provides computational efficiency and a separation between the hard-core sphere and the attractive well. The integrated version of the Lennard-Jones is proposed to approximate the interaction of a single, small bead with a bigger entity (half space filled with Lennard-Jones interaction centres) represented by the nanoparticle, about an order of magnitude larger [Israelachvili (1998)].

In this way we are mixing two different approaches. From one side we have soft potential that acts between the beads of the amphiphiles and, on the other side, we consider a harsh repulsion between beads and nanoparticle. The presence of the singularity caused problem in the large time step used in the DPD method. The simulation were not stable in temperature and some particles, during the integration of the equation of motion, could be placed beyond the singularity into the non physical region. It was hence necessary to decrease the time step of the simulation and redefine the interaction in a way that

$$U(r) = \begin{cases} -100r + 1000(1 + 0.6r_{hc}) & \text{if} \quad r < 0.6r_{hc} \\ h\Big(\Big(\frac{r_{hc}}{r}\Big)^9 - \Big(\frac{r_{hc}}{r}\Big)^3\Big) & \text{if} \quad 0.6r_{hc} < r < 3r_{hc} \\ 0 & \text{if} \quad r > 3r_{hc} \end{cases} \tag{1.46}$$

Thermostat

The molecular dynamics simulations are based on the conservation of the energy but for the experimental condition is always easier to keep the temperature constant. We should hence change our thermodynamical variables from the microcanonical ensemble, NEV, to the canonical ensemble NVT. As in the case for DPD, we add two force that, following the fluctuation-dissipation theorem, termalize the system and every derived quantity will be described in unit of temperature, $k_BT = 1$. The thermostat we use stems from the Langevin description.

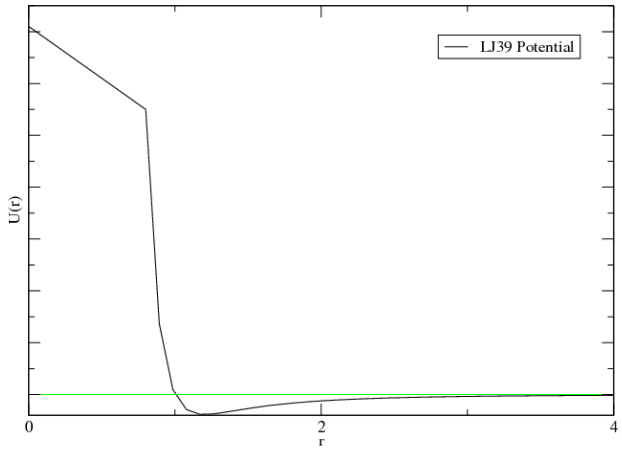

Figure 1.4: Schematic representation of the potential used, the potential presents an attractive part within the cut-off distance and the hard-core sphere radius and a repulsive potential that is smoothed around the singularity.

Langevin description

The nanoparticle, as a mesoscopic particle, requires a Brownian noise that describes the interaction with the solvent particles that, stochastically, interact with the nanoparticle. The Brownian noise implies a dissipation term that must satisfy the fluctuation-dissipation theorem. Following the Langevin equation [Orlandini (2008)] we estimate the strength of the interaction in this way.

$$m\dot{\boldsymbol{v}} = \boldsymbol{F}^c - \gamma\boldsymbol{v} + \boldsymbol{F}^g(t) \tag{1.47}$$

F^c conservative force
F^g stochastic Gaussian force
γ dumping term

The statistical average of the random forces must be zero

$$\langle \boldsymbol{F}^g(t)\rangle = 0 \tag{1.48}$$

If we describe the nanoparticle in a thermal bath in equilibrium the random forces should be a stationary process which does only depend on time differences

$$\langle F^g(t_1)F^g(t_2)\rangle = \langle F^g(t)F^g(t+\tau)\rangle \tag{1.49}$$

t_1, t_2 arbitrary times
t, τ another set of arbitrary times

If we assume that the time step of our simulation is larger than the correlation time of the Langevin force we can consider the limit that the process is uncorrelated

$$\langle \boldsymbol{F}(t_1)\boldsymbol{F}(t_2)\rangle = m^2\sigma^2\delta(t_1 - t_2) \tag{1.50}$$

m mass of the particle
σ variance of the random noise

Following [Orlandini (2008)] we can integrate the differential equation with the velocities and obtain:

$$\lim_{t\to\infty}\langle v(t)^2\rangle = \frac{\sigma^2}{2\gamma} \tag{1.51}$$

$\langle v(t_1)v(t_2)\rangle = \langle v(t)^2\rangle$ in a stationary fluid

Following the equipartition theorem

$$\lim_{t\to\infty}\frac{1}{2}m\langle v(t)^2\rangle = \frac{1}{2}m\frac{\sigma^2}{2\gamma} = \frac{1}{2}k_BT \qquad \sigma^2 = \frac{2\gamma k_BT}{m} \tag{1.52}$$

In this way we can write the coefficients that describe the Brownian dynamics for the nanoparticle

$$\frac{\Delta \boldsymbol{v}}{\Delta t} = \frac{\boldsymbol{F}^c}{m} - \gamma \boldsymbol{v} + \sqrt{\frac{2\gamma k_B T}{m \Delta t}} \boldsymbol{g}(t) \tag{1.53}$$

$\boldsymbol{g}(t)$ Gaussian noise $\langle g(t_1) g(t_2) \rangle = \delta(t_1 - t_2)$

The factor $1/\sqrt{\Delta t}$ is proper to the Wiener process and absorbs the factor that comes from the integration of the random noise for which holds $\langle g(t) g(t') \rangle = \delta(t - t')$.

Damping term

One of the most important parameter in our study is the radius of the nanoparticle and, following the Stokes law, we expect that the damping term which describes the friction with the solvent depends on the radius of the nanoparticle but not on its mass. That suggest us to define the damping term, γ, in the following way

$$\gamma := \frac{6\pi \eta r_{hc}}{m} \tag{1.54}$$

η is a viscous term in units of $[m/s^2]$
$2r$ nanoparticle's diameter

where η is the viscosity, and m the mass. The viscosity term is connected with the relaxation time of the system and, hence, with the dynamics of the system. The change of the viscous term by the radius will change the temporal scale of the dynamics of the nanoparticle but since we are not interested in such a property the exact determination of the viscosity, η, is not important as long as the balance within the random and the conservative forces is correct.

Chapter 2

Mapping

In this chapter we want to configure the system to represent a specific experimental set-up. We briefly discuss which are the quantities that we can extract from the simulation that can be compared to experiments. At the beginning we estimate the way to map the particular experimental set-up by quantifying the interaction of the nanoparticle in the membrane in terms of contact angle, surface tension and chemical potential.

2.1 Macroscopic Quantities

A molecular dynamics simulation consists in calculating the forces that act between the particle and integrate the equation of motion. The results of our simulations should be expressed in terms of macroscopic quantities, i.e. tangential pressure, bending rigidity of the plane, surface tension, diffusion constant, viscosity... This estimation serves to identify time, length, and energy scale to compare simulated and experimental system.

Length Scales

The length scale is defined by the end-to-end distance, R_e, of the amphiphiles. This is a suitable quantity because both the chain size and the number of molecules in a volume R_e^3 does not depend on the chain discretisation. The statistical length of a single monomer in a polymer is a quantity discussed in literature and it depends on the solvent. For example the statistical length for a monomer of polybutadiene is $0.66[nm]$ in [Mark (2007)], while is $0.55[nm]$ in [Ch. M. Papadakis (2006)]. Due to the rigidity of the membrane the density profile in the direction normal to the surface shows narrow interfaces that confine the hydrophobic melt in the interior. In this way a definition of the thickness of the membrane can be provided.

Energy Scales

Different energies characterise a membrane. Each polymer adheres to the others via a vaporisation energy, i.e. the energy required to remove one chain from the system at the liquid-vapour coexistence. The chemical potential is the free energy that depends on the temperature quantify the cost of adding or removing a chain. There are also two important macroscopic properties of the membrane that can be easily obtained experimentally, the bending rigidity and the surface tension of the membrane. To calculate these two parameters we can conceive the membrane as an elastic sheet. In every point of this sheet we can build two osculating circles in the direction perpendicular to the normal of the plane. The radii of these circles are related to the mean and Gaussian curvature. The energy, of a fluctuating and curved sheet depends on the local deformation of the surface and is quantified by the Helfrich Hamiltonian,[Helfrich

(1978)], as defined in [Farago and Santangelo (2005)]

$$H = \int \mathrm{d}x\mathrm{d}y\Big(\frac{\Sigma}{2}(\nabla z(x,y))^2 + \frac{k_{br}}{2}(\nabla^2 z(x,y))^2\Big) \tag{2.1}$$

where the function $z(x,y)$ is the position on the normal of the surface for the point of coordinates (x,y) where k_{br} is the bending rigidity and Σ the surface tension.

Time Scales

We have a rather reliable estimate of the length scale of the system but the time scale is a more delicate issue. A common practice to define a time scale is to estimate the self-diffusion coefficient of the amphiphiles or the shear viscosity. For example [Shillcock and Lipowsky (2007)] compared the time scale of the simulation with the experimental value of the diffusion coefficient of the lipids in a planar membrane and found that the fusion process of a vesicle into a membrane last between 160 and 480 $[ns]$, which is compatible with the experimental data.

The time scale of the dynamics is regulated by the mass of the beads and the viscosity that defines the temporal evolution of the system. To build a reliable control on the dynamics of the system we should estimate a mass for each type of bead that depends on the discretisation. Every different region in space should have a different viscosity that has to be estimate. We would need to introduce the mass of the nanoparticle that depends on the geometrical configurations in case of non symmetrical or fluctuating shape. Moreover, the nanoparticles, that have a radius of the core much smaller than the radius of the polymeric brush, are described as star polymer. The chains of the hydrophobic monomers and the brush can anchor themselves and increase the friction.

The use of the TEM instrumentation to visualise the nanoparticle requires a low temperature to reduce the thermal noise. From the synthesis to the visualisation, the dynamics of the nanoparticle is completely lost and no information came from the experimental side. The estimation of a temporal scale is out of the scope of this thesis and we focus our interest on equilibrium properties.

Dynamics & Equilibrium

Our chief goal is in fact to determine equilibrium configuration of the nanoparticle. To determine the equilibrium properties the mass is not important. If we look at the Boltzmann distribution, since the potential does not depend on the velocities, we can integrate the momentum in the phase space and obtain the thermal length that will disappear in the averages.

$$f_B(V,T) = \frac{1}{N!h^{3N}}\int \mathrm{d}\mathbf{\Gamma}_i e^{-\sum_i^N \frac{mv_i^2}{2k_BT} - \sum_j^N \frac{U(r_i,r_j)}{k_BT}} = \frac{1}{\Lambda^{3N}}\int \mathrm{d}\boldsymbol{r}_i e^{-\frac{\sum_j U(r_i,r_j)}{k_BT}} \tag{2.2}$$

$\mathbf{\Gamma} = (\boldsymbol{p}, \boldsymbol{r})$
$\Lambda^{-}1 = \sqrt{2\pi m k_B T/h^2}$ thermal length

where we have introduce the De Broglie thermal length

$$\Lambda^{-1} = \sqrt{\frac{2\pi m k_B T}{h^2}}$$

Even the time is not important in our simulation since we do not want to scale the evolution of the system.

2.2 Configuring the System

The specific experiment we refer to is realised by [W.Müller *et al.* (2008)] where a solution of amphiphilic polymers self assembly in ordered structures. The composition investigate is poly(butadiene)-b-poly(ethylene oxide)-hg that for brevity we denote $PB_n - PEO_m - hg$. The monomers of butadiene have an non-polar nature, the ones of ethylene oxide are miscible in water and in methanol. Blocks of both types

of monomers are joint to form an amphiphilic block copolymer. These amphiphiles have at the last monomer of ethylene oxide an head group that is in this case an hydrogen atom, H, or a succinic anhydride molecule, $COOK$. In this paper a detailed analysis is performed to build a phase diagram that distinguish between the self-assembly into vesicles, cylinders or micelles. The analysis shows that the formation of structures depends on the the block ratio, the block length, the solvent and the PEO-sided end group. The work reports that the only structures that create stable bilayer in form of micelles are realised by the composition of $PB_{130}-PEO_{66}-COOK$, $PB_{130}-PEO_{66}-H$. This configuration is the reference point for the simulations. During the formation of the vesicles the same author, [Maskos (2006)], could introduce in the solution a hydrophobic fluorescent dye called nile red, widely use for imaging purpose since many years [Fowler *et al.* (1987)], and highly fluorescent quantum dots.

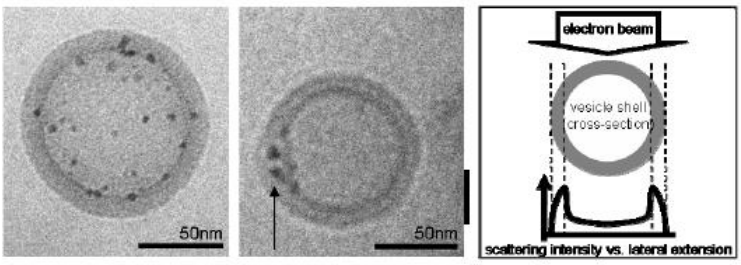

Figure 2.1: a), b) Cryogenic TEM images of quantum dots loaded vesicles in aqueous solution. c) Schematic drawing: TEM scattering intensity vs. lateral extension [W.Müller *et al.* (2008)].

Using cryogenic TEM and fluorescent microscopy, (Fig: 2.2) , was observed the presence of the nanoparticles in the hydrophobic shell. The resolution of the TEM instrumentation permits to obtain important information on the position of the substrates in the shell. The hydrophobic shells have a mean thickness of $16[nm]$ and the radius of the formed vesicles have a very broad distribution in diameter. The smallest vesicles have a diameter of hundred of $[nm]$ while the biggest of several μm. The hydrophobic substrates encapsulated have a diameter of $5.7 \pm 0.6[nm]$ for the quantum dots and other hydrophobic load that can be stable in the membrane range between 3 and $9[nm]$.

With the data furnished from this experimental group we are going to configure the system for the simulations.

Mapping the virial coefficients

Our model take into account three external parameters to set the initial virial coefficients. We begin by estimating the density of coexistence. The composition of monomers in a single chain is

$$PB_{130} - b - PEO_{66} - \mathrm{hg} \tag{2.3}$$

The composition of the hydrophobic tail is a sequence of 130 monomers of butadiene and the hydrophilic head group is composed by 66 monomers of ethylene oxide.

The molar mass of a monomer of butadiene is $m_m = 52[g/mol]$, for a monomer of ethylene oxide is $m_m = 44[g/mol]$. The molar mass of the complete molecule is $m_m = 9666[g/mol]$. Referring to [Mark (2007)] the statistical length of a butadiene monomer is $l_B = 0.66[nm]$ and of a ethylene oxide is $l_{EO} = 0.72[nm]$. The end-to-end distance of an ideal Gaussian chain of the same structure is $R_e = \sqrt{l_B^2 N_B + l_{EO}^2 N_{EO}} = 9.531[nm]$. A typical density of mass for an polymer melt is $\rho_p = 1[g/cm^3]$. In units of R_e the

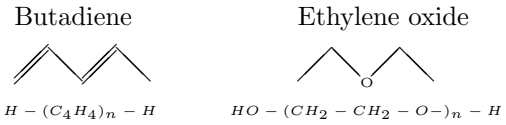

Figure 2.2: Chemical structure of the single monomer of butadiene and ethylene oxide

density of chains per unit volume is $\rho_c = 42.5[chains/R_e^3]$. The density of chains is

$$\rho_c = \frac{N_c}{V} = \frac{\rho_p N_A}{m_m}\Big[\frac{g}{g\text{cm}^3}\Big] = \frac{\rho_p N_A}{m_m}\frac{1}{10^{21}}\Big[\frac{1}{\text{nm}^3}\Big] = \frac{\rho_p N_A l_m^3}{m_m}\frac{N_b^{\frac{3}{2}}}{10^{21}}\Big[\frac{1}{R_e^3}\Big]$$

where N_A is the number of Avogadro and l_m is the statistical length of the molecule expressed in nano-meters.

Flory-Huggins Parameter

The Hamiltonian of interactions expressed in (1.24) is invariant for the coarse-grained operation, i.e. changing the discretisation of the molecular contour for a particular system, ρ_0 fixed, the quantities $\chi\rho_0$ and $k\rho_0$ are invariant and that means that the system should have the same incompatibility and the same cohesive energy per unit volume. If we conserve the number of chains the parameters χN_b and kN_b are invariant.

We introduce the energy of vapourisation, ΔE_A, that is the sum of all the energy that interact with a certain molecule A that has to be disrupted if we want to remove the molecule form the system. The vapourisation energy divided by the volume of the molecule is the cohesive energy density which is directly connected with the interaction energy of system of one species, A, namely

$$-\frac{u_{AA}}{2} = V_c\frac{\Delta E_A N_A}{V_A} \tag{2.4}$$

where the vapourisation energy is defined positive while the interaction energy v_{AA} is negative. Hildebrand and Scott introduced the solubility parameter defined as $\delta_A^2 := \Delta E_A/V_A$ that allow us to define the χ parameter in terms of the solubility

$$\chi \simeq V_c\frac{\delta_A^2 - 2\delta_{AB} - \delta_B^2}{k_B T} = \frac{V}{N_c N_b k_B T}(\delta_A - \delta_B)^2 \tag{2.5}$$

The Hildebrand parameter is a well-known quantity in case of monomers in solution and the values are provided in literature [Mark (2007)]. In the case of polymers the solubility of a single monomer in the chain is difficult to estimate and is provided from experimental and theoretical calculations. In this case we refer to [Mark (2007)] for the poly-butadiene, $\delta_B = 16.2$ (experimental) and for the poly-ethyleneoxide $\delta_{EO} = 20.2$ [Chung *et al.* (1997)]. We therefore obtain a χN parameter

$$\chi N_b = \frac{(\delta_B - \delta_{EO})^2}{k_B T}\frac{V}{N_c} = 60.803 \tag{2.6}$$

This is only a rough estimate because of significant uncertainties of the solubility parameters in the literature. The estimation of these quantities is rough, some quantities are imprecise and the values reported in literature can disagree. All the interactions depend on the input parameters and we must in any case define reasonable virial coefficient.

2.2.1 Incompatibility

The incompatibility between the two species causes the amphiphiles to stretch and changes the surface per chain, S_c, and the thickness, d_t, of the hydrophobic shell. To measure the changes of these two parameters for a fixed density we run a simulation for different values of χN in the NP_tT ensemble. In this ensemble the distance between walls of the box changes to keep the tangential pressure constant.

χN	d_t $[R_e]$	S_c $[R_e^2]$
30	0.826	0.0197
40	0.834	0.0186
50	0.92	0.0150

The values $\chi N = 20$ and $\chi N = 60$ did not result in stable bilayers. The properties for the other values of χN are compiled in the table below.

Another way to obtain the thickness of the hydrophobic shell is to simulate a box with a small extension with respect to the equatorial plane of the membrane and a large extension in the other directions. The two-dimensional membrane spans the periodic boundary conditions in one direction but it creates a free edge along the other direction.

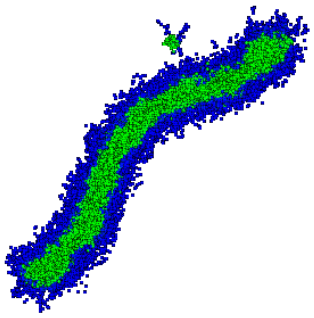

Figure 2.3: Membrane with free edges.

If the membrane does not have vanishing surface tension it will contract or bend to find the best configuration, a tensionless state.

In the last graph, (Fig: 2.2.1), we can see how the thickness of the hydrophobic beads increase as we increase the incompatibility χN.

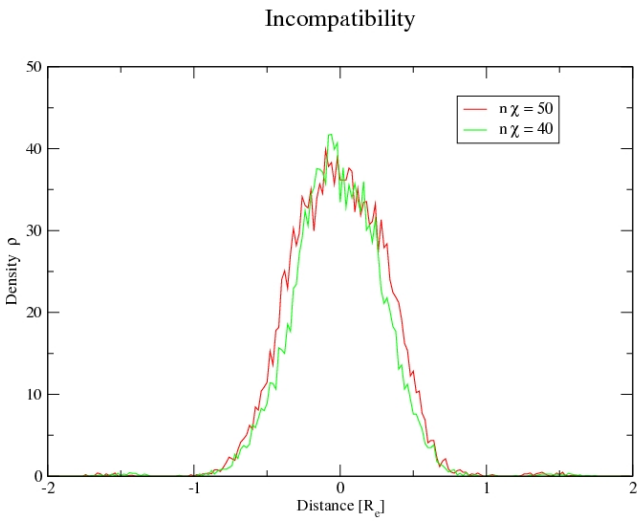

Figure 2.4: Density profile of the hydrophobic beads. The thickness of the hydrophobic layer increase by increasing the incompatibility between the two species.

2.3 Mapping the Nanoparticle

As mentioned before, the definition of the quantities that describe the nanoparticle should be compared with the effects that they produce, i.e. the strength of interaction define the miscibility of the particle in an non-polar solvent. In the following sections we provide a quantification of the effects that characterise the interaction between nanoparticle and membrane.

2.3.1 Surface Tension

The homopolymer melt is attracted to the nanoparticle for distances between the hard-core radius and the cut-off distance. The presence of an hard wall would cause a repulsive force for the loss of conformational energy and near the wall we observe a depletion in the density connected with the Edwards correlation length and the incompressibility as shown in the previous chapter. The hard core repulsion competes with the attraction and the easiest way to calculate the surface tension is to define the nanoparticle as a wall that interact with a homopolymer melt. The simple geometrical calculation simplifies the calculation of the stress tensor that in orthogonal coordinates is diagonal. The first system that we consider is a homopolymer bulk connected by periodic boundary condition in the x and y directions. The system in this configuration will assume a parallelepiped shape with two free faces in the z direction. On the upper face we approach a wall that will repel the bulk within its hard core part and will approach it in its attractive part causing an increasing in the density of the wall.

The surface tension in calculable via the pressure tensor

$$\Sigma = \frac{1}{2l_z}\Big(P_{zz} - \frac{1}{2}\Big(P_{yy} + P_{xx}\Big)\Big) \tag{2.7}$$

Where the pressure is calculable by:

$$P_{dd} = \frac{1}{2}m\sum_{i}^{N}(v_i^d)^2 + W_{dd}/V \qquad 1 \leq d \leq 3 \tag{2.8}$$

$W_{dd'} = \sum_{ij}^{N} F_{ij}^{d} r_{ij}^{d'}$ Virial
V Volume

that permits to determine the dependence of the surface tension on the Hamaker constant. The virial, as defined in (1.8), is the sum of the total forces acting on a

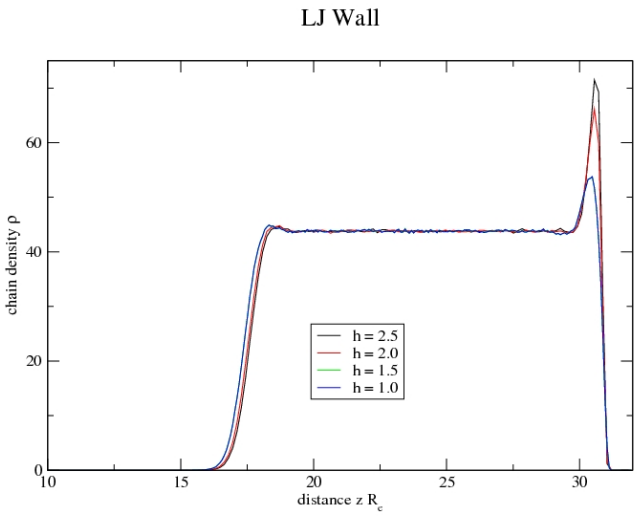

Figure 2.5: Homopolymer melt attracted by a Lennard Jones wall for different Hamaker constants

particle.

$$\begin{aligned}\sum_i \boldsymbol{r}_i \boldsymbol{f}_i^{tot} &= \sum_i \boldsymbol{r}_i (\sum_{j\neq i} \boldsymbol{f}_{ij} + f_i^{ext}) = \sum_i \Big(\frac{1}{2} \sum_{j\neq i} (\boldsymbol{r}_i \boldsymbol{f}_{ij} + \boldsymbol{r}_j \boldsymbol{f}_{ji}) + \boldsymbol{r}_i \boldsymbol{f}_i^{ext} \Big) = \\ &= \sum_i \Big(\sum_{j>i} \boldsymbol{r}_{ij} \boldsymbol{f}_{ij} + \boldsymbol{r}_i \boldsymbol{f}_i^{ext} \Big) \end{aligned} \tag{2.9}$$

Where $\boldsymbol{f}^{ext}$ is the force added by the wall, $\boldsymbol{f}_{ij}$ and $\boldsymbol{r}_{ij}$ are the mutual distances and forces.

Contact angle

If we consider a melt of interactive particles the particles in the bulk will feel the interaction with the other particles in any direction. On the surface half space of interaction is missing and the forces will likely pull the particle to the interior. This means that it costs energy to have particles on the surface and the system will minimise its surface area. A homopolymer melt in the solvent would tend to assume a spherical shape. If the sphere approaches to an attractive wall it creates a sharp edge parallel to the wall and increases its surface. In this case the surface is increased thanks to the additional forces that the wall add to the system. At equilibrium the system balances the strength of the surface tension at the contact line between the three interfaces: vapour/solid, vs, liquid/solid, ls and liquid/vapour, lv. The Young formula quantifies the contact angle θ_c

$$\Sigma_{vs} - \Sigma_{ls} - \Sigma_{lv} \cos(\theta_c) = 0 \tag{2.10}$$

v vacuum
s solid
l liquid
θ_c Contact angle

The surface tension between the vacuum and the solid is obviously zero and the determination of the contact angle will provide us with an estimate of the ratio between the surface tensions.

If we consider a spherical system (an oil drop) we can calculate the surface tension assuming that the drop would conserve a spherical shape. In this way, we can retrieve information about the volume of the drop (i.e. the number of particles) and the centre of mass in the z direction. Simple geometrical calculations give us the following formulae

R Sphere's radius
z_{cm} centre of mass for the zeta coordinate

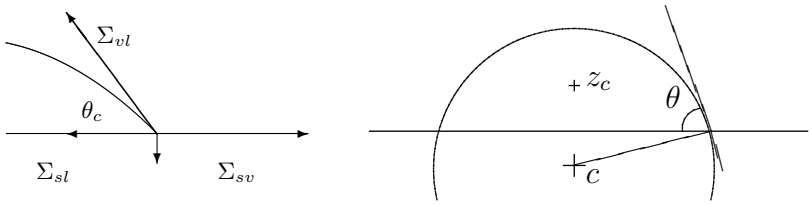

Figure 2.6: Representation of the balancing of the forces that determines the contact angle and visualisation of the centre of mass of a drop in contact with the wall.

$$V = \pi R^3\Big(\frac{2}{3} - \cos(\theta_c) + \frac{\cos^3(\theta_c)}{3}\Big) \qquad V z_{cm} = \frac{\pi R^4}{4}(1 - \cos^2(\theta_c))^2 \tag{2.11}$$

This yields a non invertible equation whose roots can numerically calculated.

$$f(\theta; V, z_{cm}) = \Big(\frac{V}{\pi}\Big)^{1/3}\Big(\frac{3}{2 - 3\sin(\theta) + \sin^3(\theta)}\Big)^{3/4}\cos^4(\theta) - z_{cm} \stackrel{!}{=} 0 \tag{2.12}$$

This function provides, in the interval between $[0, \pi]$, two roots symmetrical to $\pi/2$ and the picture will help us to exclude one of the two roots. The determination of the z coordinate for the contact surface is set to r_0, the point in which the Lennard Jones potential is zero. There are also a few particles in the hard-core region due to the large integration step of the velocity Verlet algorithm but we neglect its importance. The beads presents within the hard core distance and the position of the wall are typically a fraction of 0.1 % of the total particles and do not cross more the 1/10 the hard core radius. Here we present a table where a comparison between the Hamaker constant of the interaction is compared to the contact angle of an oil drop. In the following

Hamaker h	Contact angle
2.5	80.44
2.0	91.64
1.5	108.85
1.0	136.5

picture we show a circular interpolation of the surface of the drop that is attracted to the wall. From the graph one can see the decreasing of the contact angle at decreasing Hamaker constant.

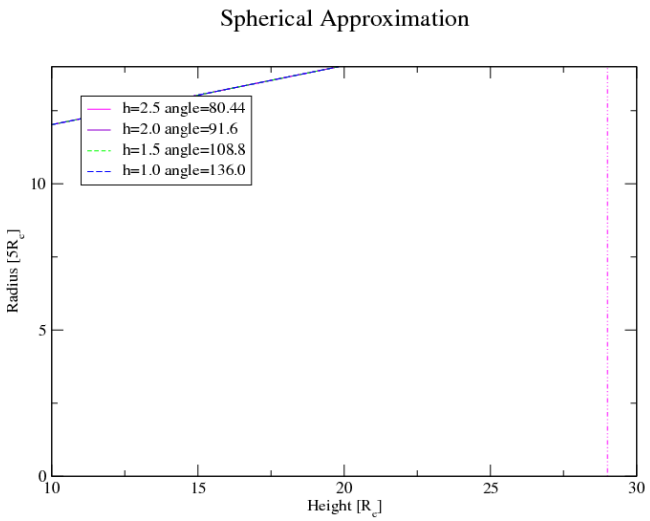

Figure 2.7: Radial distribution of density for calculating the contact angle between a Lennard-Jones wall with an Hamaker constant of 2.5 and a sphere melt. Only the shell is visualised

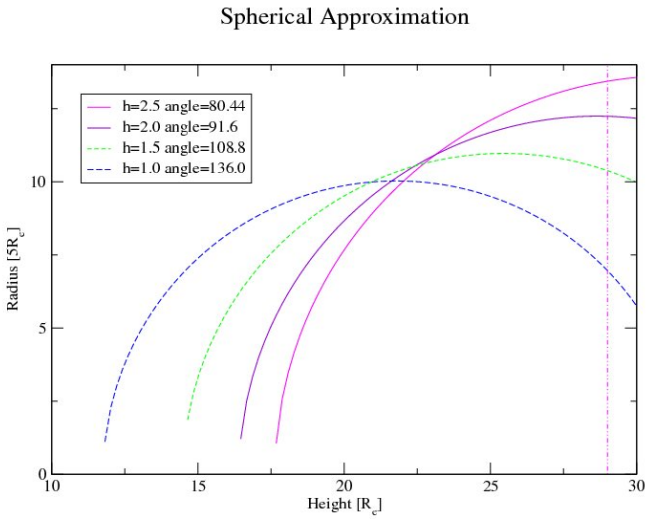

Figure 2.8: Estimation of the contact angle depending on the Hamaker constant of the wall. Each line represents a different interaction

2.4 Chemical Potential

One useful parameter for studying the properties of a system is the chemical potential that allows us to calculate the difference in free energy respect to the nanoparticle. The Gibbs free energy of a system is the sum of three terms

c number of components

$$F = TS - PV + \sum_{i=0}^{c} \mu_i N_i \tag{2.13}$$

The excess chemical potential is defined as the cost necessary to add one particle to the system and can be calculated as the partial derivative of the free energy respect to the number of particle.

$$\mu = \left(\frac{\partial F}{\partial N}\right)_T \tag{2.14}$$

In this case we want to calculate the excess chemical potential express in term of the size of the nanoparticle. The difference in free energy for a nanoparticle with a radius r_{hc} and r'_{hc} is

$$\Delta F = -k_B T \ln \frac{\sum_i^{N+1} e^{-\beta U_p} e^{-\beta U_{np}(r_{hc})}}{\sum_i^{N+1} e^{-\beta U_p - \beta U_{np}(r'_{hc})}} = \tag{2.15}$$

$$= -k_B T \ln \frac{\sum_i^{N+1} e^{-\beta U_p} e^{-\beta (U_{np}(r'_{hc}) - \Delta U_{np})}}{\sum_i^{N+1} e^{-\beta U_p - \beta U_{np}(r'_{hc})}} = -k_B T \ln \langle e^{-\beta \Delta U_{np}} \rangle \tag{2.16}$$

where $\Delta U_{np} = U_{np}(r_{hc}) - U_{np}(r'_{hc})$. If we suppose an infinitesimal increasing of the radius we write

$$\Delta U_{np} = \frac{\mathrm{d}U_{np}}{\mathrm{d}r_{hc}} \Delta r_{hc} \tag{2.17}$$

The partial derivative of the free energy respect to the nanoparticle radius is

$$\frac{\partial F}{\partial \Delta r_{hc}} = -k_B T \frac{\partial}{\partial \Delta r_{hc}} \ln \langle e^{-\beta \frac{\mathrm{d}U_{np}}{\mathrm{d}r}} \rangle = -k_B T \left\langle \frac{\mathrm{d}U_{np}}{\mathrm{d}r_{hc}} \right\rangle \tag{2.18}$$

where the last term is the average on the ensemble.

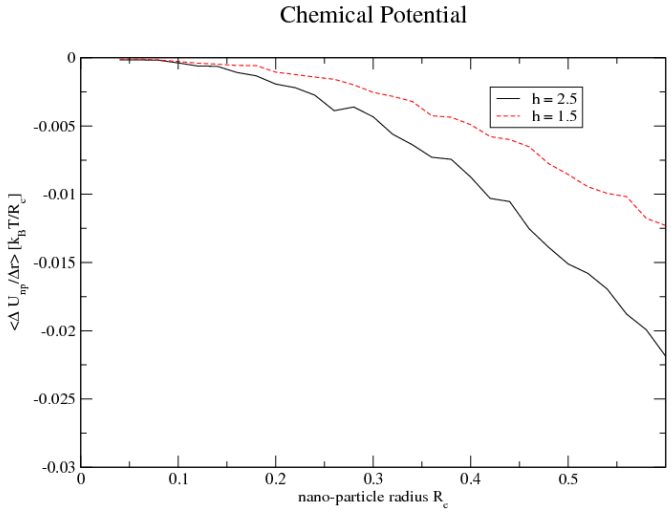

Figure 2.9: $\langle \Delta E / \delta r_{hc} \rangle$ depending on the r_{hc} radius of the nanoparticle and two different Hamaker constants.

Chapter 3

Building the Stability Diagram

The model that we described in the previous chapters has been devised to study the properties of the system membrane/nano-particle. In this chapter we are going to present the results of the simulations.

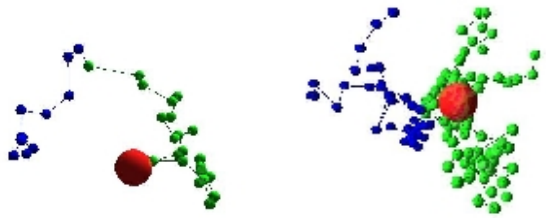

Figure 3.1: Attraction of the nanoparticle by a surrounding chain. To the left a hydrophobic bead is attracted by the short range potential of the nano-particle, on the right hand side a stronger potential attract the hydrophobic beads. The nanoparticle (red) and the hydrophobic beads (green) are in the hydrophobic layer of the membrane, the hydrophilic beads (blue) on the left compose the outer layer. The plane of the membrane is normal to the view.

To introduce the nanoparticle into a membrane we arrange the chains placing the hydrophobic beads within two planes at a distance d_t which is obtained in the previous chapter for the tensionless state. At the centre of the simulation box we create a hole where no beads are present and collocate the nanoparticle. Once the system is equilibrated we can vary the Hamaker constant and the radius of the particle.

One of the most important information about the equilibrium of the system relates to the stability of the nanoparticle in the two leaflets of the membrane. For different values of the radius of the nanoparticle and the Hamaker constant we observed when the nanoparticle remained in the membrane or was expelled. In the (r_{hc}, h) plane, we built a stability diagram showing which values provide a stable configuration. Before to show the stability diagram we consider the interactions between the beads and the nanoparticle. A competition between different potentials influences the stability of the nanoparticle.

The nanoparticle size increases the number of interactions, especially the attractive ones, but it also deforms the elastic leaves of the bilayer membrane. From the Helfrich Hamiltonian, (2.1), the bending of a membrane costs of energy and the membrane may prefer to assume a flat shape expelling the nanoparticle. Moreover, the beads along the amphiphiles are connected to each other via bonds and the presence of the nanoparticle

obliges the chains to bend themselves around it. The excluded volume and the loss of conformational energy compete with the attractive part of Lennard-Jones potential. In the following section we show some phenomenological considerations on the system.

3.1 Excluded Volume

The integral of the Mayer function, (1.42), defines the excluded volume which depends on the hard core of a sphere and on the type of interactions. We have calculated the radial density profiles respect to the nanoparticle position during different time periods. As we can see from the figure, (Fig: 3.1), the shell of the nanoparticle is enriched in

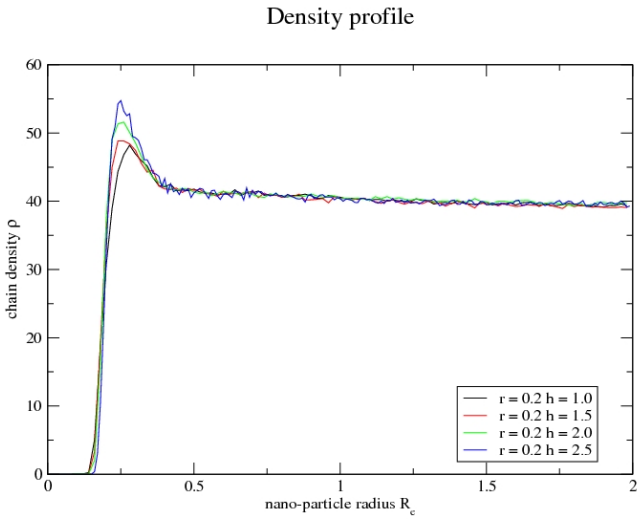

Figure 3.2: Radial density profile for a nanoparticle with radius 0.2 R_e

hydrophobic beads. The shape of the density profile decays within the cut-off radius of the interaction with the nanoparticle and does not show any oscillation shich would be typical for a solid (or gel) phase. From the figure, (Fig: 3.1), we can notice the enrichment in beads due to the number of interaction. Increasing the radius, r_{hc}, the spherical corona of the attractive well of the potential increases by a factor of $((3r_{hc})^3 - r_{hc}^3)$, where $3r_{hc}$ is the cut-off distance of the Lennard-Jones interactions. The potential energy added to the system depends also on the radius. The excluded volume increases because of the larger hard core repulsion and decrease because of the increment of the attractive interactions.

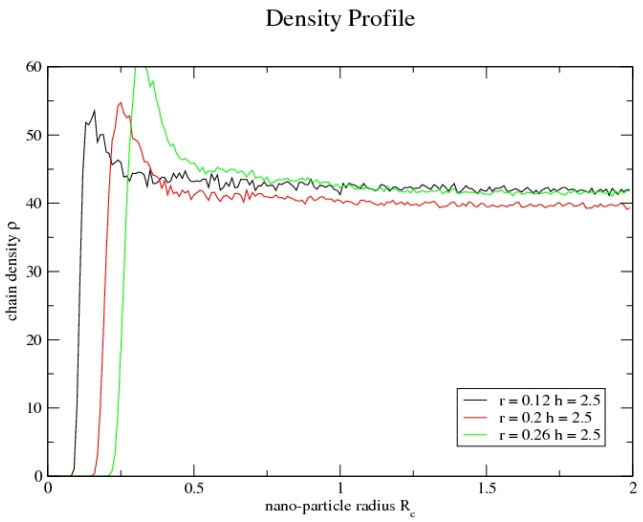

Figure 3.3: Radial Density profile for a nano particle with a Hamaker constant $h = 2.5$.

3.2 Displacement

For every simulation we monitored the position of the nanoparticle with respect to the membrane. In (Fig: 3.4), we show a long-time average of the density profile calculated along the normal to the surface of the membrane.

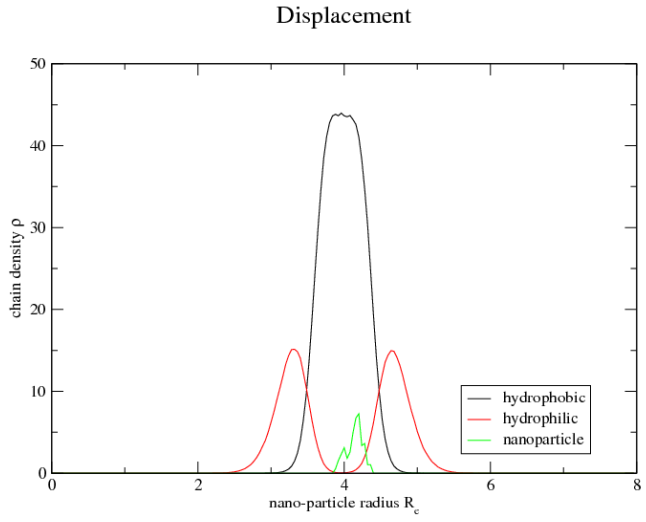

Figure 3.4: Average position of a nanoparticle defined by $h = 2.5, r = 0.26$ in a membrane.

The black line shows the density of the hydrophobic beads while the red the density of the hydrophilic. In the case of the nanoparticle the green line is not the density, since the nanoparticle is one, but the cumulative sum of the position of the nanoparticle referred to the centre of mass of the system.

In the following pictures we present a two dimensional density profile where on the abscissa is plotted the distance from the centre and on ordinate the position along the normal of the membrane, z. The reference point to calculate the radial distance can be the position of the nanoparticle, (np,np,np), the position of the centre of mass of the membrane, (cm,cm,cm), or the position of the centre of mass of the membrane for the z coordinate and the position of the nanoparticle for the x and y coordinate, (np,np,cm). Every picture represents an average over many time periods. The first sequence of pictures, (Fig: 3.2), show the displacement for small radius. The green colour represents the apolar beads while the blue the polar ones. The more the colour is bright the more the density is high. The nanoparticle is represented by the red colour and has for the previous graph, (Fig: 3.4), the red dots are represent the position of the nanoparticle.

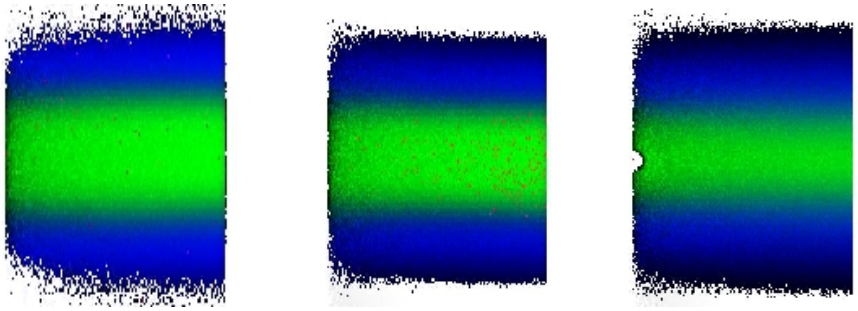

Figure 3.5: Averaged density profile of the nanoparticle in the membrane. From left to right: a) Reference frame (cm,cm,cm) of the system in which a small nano-particle ($r = 0.1$,$h = 1.0$) exit from the membrane, b-c) a slightly bigger nano-particle ($r = 0.12$, $h = 2.0$) that is confined in the membrane. In b) is respect the (cm,cm,cm) centre, in c) respect to (np,np.np).

The smallest particle in (Fig: 3.2), exits from the shell while a slightly bigger particle is stable. The nanoparticle rapidly diffuses in the membrane and does not bend the leaflets.

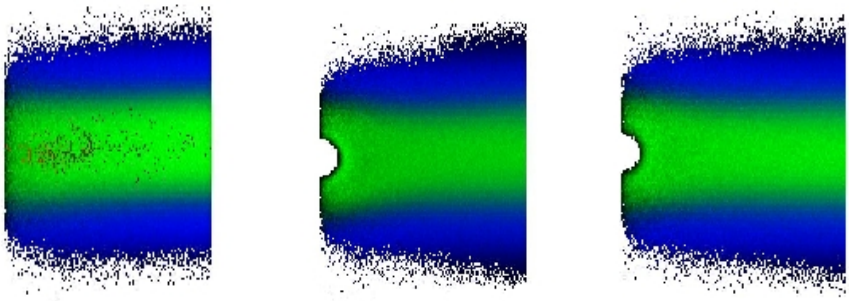

Figure 3.6: a) (cm,cm,cm) frame for a ($r = 0.2$, $h = 2.5$) nano-particle. b) (np,np,np) for a ($r = 0.2$, $h = 2.5$) and a c) ($r = 0.2$, $h = 1.0$) (np,np,np)

The next sequence, (Fig: 3.2), shows a medium size stable particle. The movement is confined in the plane parallel to the leaflets and the particle does not approach to the hydrophilic head group region. The bending of the leaves becomes visible.

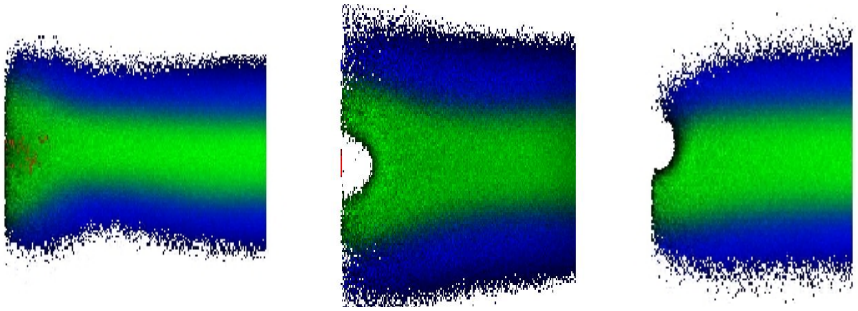

Figure 3.7: a) a ($r = 0.34$, $h = 1.0$) nano-particle that in the reference frame (cm,cm,cm). b) a slightly smaller ($r = 0.3$, $h = 1.0$) that deforms the membrane in its neighbourhood and in the (np,np,cm) frame and in c) the same nano-particle ($r = 0.3$, $h = 0.25$) with a lower interaction strength that can it would be repelled by the hydrophobic interior but it can not cross the hydrophilic layer due to the repulsion with the beads.

The diameter of the nanoparticle in, (Fig: 3.2),is now comparable with the thickness of the membrane and in figure, (Fig: 3.2) we can see a considerable bending of the leaves. In the last picture the nanoparticle is block near to one leaf and can not cross the repulsive wall created by the hydrophilic beads.

3.3 Stability diagram

The simulation results for different values of h and r_{hc} are compiled in a stability diagram. In the graph are shown the condition for the stability.

It is important to notice some points in the stability diagram, (Fig: 3.3). There is a particular configuration where the equilibrium is indifferent, i.e. the nanoparticle moves all around the system box and can go beyond the hydrophilic layer, stay for some time in the hydrophobic interior and exit again. Bigger nanoparticles caused instead the rupture of the membrane because the spherical corona of the potential well attract a large number of hydrophobic beads. The depletion created on the equatorial plane around the nanoparticle is filled by the closest chains that stretch themselves and in some cases drag the hydrophilic block in the interior. This provokes the formation of a micelle around the nanoparticle and a consequent rupture of the membrane. The fixed boundary edges of the box creates a tension in the elastic membrane. To prevent the rupture of the membrane that depends on the choice of the boundary conditions we run the simulations in the NP_tT ensemble where the distance between the edges of the box change to adopt vanishing small tangential pressure. These simulations are represented by the green stars when the rupture in the NVT ensemble happened. Bigger nanoparticles cannot in any case be stable in the membrane.

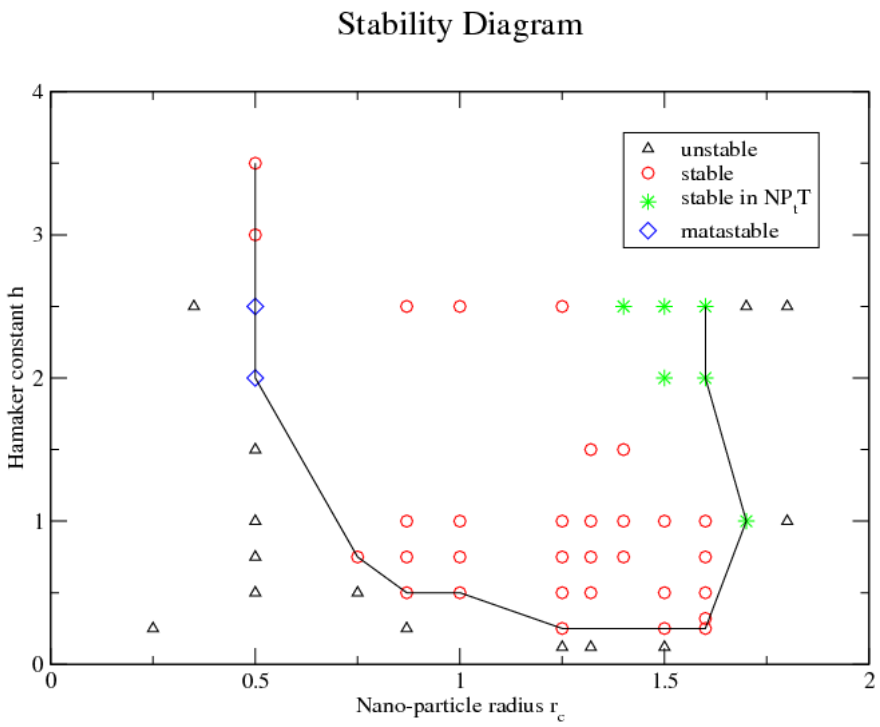

Figure 3.8: Stability Diagram of the stability of the nano particle in the membrane depending on its radius and Hamaker constant.

Another way to reduce the tension is to introduce some homopolymer chains in the shell. As observed, (Fig: 3.3) , the chain move to fill the depletion around the nanoparticle.

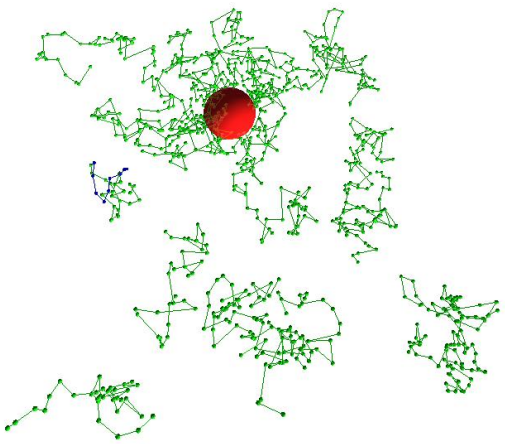

Figure 3.9: Additional homopolymer chains that fill the depletion created by the nanoparticle. In the frontal view only the added homopolymer chaisn are visualised.

Additional simulations can be run to study the change in the surface tension with the contribution of the added homopolymer and to see if the stability region with the stability diagram can be extended to larger particle sizes.

Chapter 4

Conclusion & Outlook

Summary

In this work a coarse-grained model is proposed to simulate a stable bilayer membrane where a hydrophobic nanoparticle is inserted into the hydrophobic shell. In the model the solvent particles are integrated out and the interactions between the amphiphilic molecules are calculated via an effective Hamiltonian. The modelling of the system proceed configuring the hydrophobic interactions and providing a weighing function that defines a nearly incompressible polymer melt. The friction term, the density of the system and the time step are chosen to achieve stability in temperature and computational efficiency. The hydrophilic block is added to the chain forming an amphiphilic molecule and the membrane is preassembled. The thickness and the molecular density per area is calculated for the tensionless state. The nanoparticle is defined by a Lennard Jones potential, defined by two parameters, the Hamaker constant, h, and hard core radius r_c.

To compare our results we refer to a particular experimental set-up and we aim at building a system that can be mapped onto an experimental realisation. The model depends on three parameters, the density of the chains, ρ_0, the incompressibility, κN and the incompatibility between the two species, χN. A brief explanation shows how to estimated values these quantities. The estimation of the coarse-grained parameters are obtained by comparison of key characteristics with available experimental data. Just as well, the Hamaker constant and the hard core radius that describe the nanoparticle should be expressed in terms of experimental relevant quantities. We calculate the contact angle between a plane with the same potential and a homopolymer drop is calculated.

The coarse-grained model finally permits to introduce the nanoparticle into a stable bilayer and study the equilibrium properties. The behaviour of the nanoparticle in the membrane interior is investigated and a phase diagram is obtained showing the boundary in the size of the nanoparticle that guarantees stability.

Results

The experimental values available are few and we can only have a qualitative agreement on the maximum and minimum radius of the nanoparticle. The observed quantum dots and nanoparticles stably incorporated in the shell have a diameter ranging between the $3-9[nm]$ [Maskos (2006)]. Comparing the thickness of the polymeric vesicles, $16[nm]$, with the one of the simulations we can say that the observed range for the stability is between 3 and $11[nm]$. Further experimental data should provide an estimation of the contact angle between the coating on the nanoparticles and an homopolymer of butadiene, which will allow for a better calibration of our coarse-grained model.

Unfortunately, no other experimental data are available at the moment which would allow a more quantitative comparison. Our coarse-grained model describes a class of membrane/nanoparticle system and it would be interesting to compare to experimental results that correspond to slightly different coarse-grained parameters. In particular,

the dependence on the strength of the interaction between nanoparticle and hydrophobic blocks can be varied in experiments by altering the nanoparticle's coating.

Outlook

Some other interesting physical conditions can be investigated. The vesicle can have different sizes, about two order of magnitude [Maskos (2006)], but the same thickness. The curvature of the shell is another fundamental parameter that influences the stability of the nanoparticle inclusion. Additionally, it would be interesting to explore to what extent the nanoparticle can be stabilised in the membrane by adding a small amount of hydrophobic polymers.

At the formation of the vesicles in the experiment a certain number of nanoparticles were included in the shell. The next important step would be to observe the mutual interaction within the nanoparticles and how this number can affect the stability of the system.

Acknowledgements

A particular thanks to Prof M. Müller that provided and guided this research, to M. Hömberg that furnished the fast program and many important explanations and to Dr. K. Daoulas for his help and precious advices. We are also grateful to the research group of Prof. Maskos for the stimulating collaboration and interest in our work.

Appendix A

Appendix

Velocity Verlet Algorithm

The velocity Verlet algorithm integrates the equations of motion in the approximation of infinitesimal time steps and a potential that does not depend on the velocity. The Liuville operator on the *phase* space ($\mathbf{\Gamma} = (\boldsymbol{r}_1, , \boldsymbol{r}_N, \boldsymbol{v}_1, , \boldsymbol{v}_N)$) space acts as

$$\dot{\mathbf{\Gamma}}(t) = \imath\mathcal{L}\mathbf{\Gamma}(t) \qquad \imath\mathcal{L} = \sum_i^N \boldsymbol{F}_i \nabla_{\boldsymbol{p}_i} + \frac{\boldsymbol{p}_i}{m_i}\nabla_{\boldsymbol{r}_i} \tag{A.1}$$

The solution of this differential equation defines the unitary evolution operator

$$\boldsymbol{U}(t) := e^{\imath\mathcal{L}t} \qquad \mathbf{\Gamma}(t) = \boldsymbol{U}(t)\mathbf{\Gamma}(0) \tag{A.2}$$

We want to factorise the evolution operator into a part that is comprised of derivatives with respect to the positions (position's translation) multiplied by a part that is comprised of derivatives with respect to the velocities (velocity's translation)

$$\boldsymbol{U}_x(t) = e^{t\sum_i^N \frac{\boldsymbol{p}_i}{m_i}\nabla_{\boldsymbol{r}_i}} \qquad U_v(t) = e^{t\sum_i^N \boldsymbol{f}_i\nabla_{\boldsymbol{p}_i}} \tag{A.3}$$

The Campbell-Hausdorf formula up to the first order with respect to the time step Δt yields.

$$\mathbf{\Gamma}(\Delta t) \simeq \boldsymbol{U}_p(\Delta t/2)\boldsymbol{U}_x(\Delta t)\boldsymbol{U}_p(\Delta t/2)\mathbf{\Gamma}(0) \tag{A.4}$$

The action of this operators means that if we want to update the position and the velocities of the system we proceed through the following steps:

$$\boldsymbol{r}_i(\Delta t) = \boldsymbol{r}_i(0) + \Delta t\dot{\boldsymbol{r}}_i(0) + \frac{\Delta t^2}{2m_i}\boldsymbol{F}_i(0) \qquad \dot{\boldsymbol{r}}_i(\Delta t/2) = \dot{\boldsymbol{r}}_i(0) + \frac{\Delta t}{2m_i}\boldsymbol{F}_i(0)$$

and secondly

$$\dot{\boldsymbol{r}}_i(\Delta t) = \dot{\boldsymbol{r}}_i(\Delta t/2) + \frac{\Delta t}{2m_i}\boldsymbol{F}_i(\Delta t) \tag{A.5}$$

where $\boldsymbol{F}_i(\Delta t)$ is the recalculation of the forces after the up-dated of the position at the time Δt.

Bibliography

Bibliography

Allen, M. P. and Tildesley, D. J. (1991). Computer simulation of liquids. *Clarendon Press Oxford*.

Battaglia, G. and Ryan, A. J. (2005). The evolution of vesicles from bulk lamellar gels. *Nature Materials*, pages 869 – 876.

Bermudez, H., Braman, A. K., Hammer, D. A., Bates, F. S., and Discher (2002). Molecular weight dependence of polymersome membrane structure, elasticity, and stability. *Macromolecules*, **35**, 8203.

Bermudez, H., Hammer, D., and Discher (2004). Effect of bilayer thickness on membrane bending rigidity. *Langmuir*, **20**, 540–543.

Christian, D. A., Cai, S., Bowen, D. M., Kim, Y., Pajerowski, J. D., and Discher, D. E. (2008). Polymersome carriers: From self-assembly to sirna and protein therapeutics. *European Journal of Pharmaceutics and Biopharmaceutics*, pages – .

Chung, T. C., Lu, H. L., and Ding, R. D. (1997). Synthesis of polyethylene-g-polystyrene and polyethylene-g-poly(p-methylstyrene) graft copolymers. *Macromolecules Vol.*, **30**(5), 7533.

Dass, C. R., Walker, T. L., Kalle, W. H. J., and Burton, M. A. (2000). A microsphere-liposome (microplex) vector for targeted gene therapy of cancer. ii. in vivo biodistribution study in a solid tumor model. *Drug Delivery*, **7**, 15–19.

Discher, B. M., Won, Y.-Y., Ege, D. S., Lee, J. C.-M., Bates, F. S., Discher, D. E., and Hammer, D. A. (1999). Polymersomes: Tough Vesicles Made from Diblock Copolymers. *Science*, **284**(5417), 1143–1146.

Dünweg, B. and Paul, W. (1991). Browian dynamics simulation without gaussian number generator. *Int. J. of Mod. Phy. C*, **2**(3), 817.

Espanol, P. and Warren, P. B. (1995). Dissipative particle dynamics: Bridging the gap between atomistic and mesoscopic simulation. *Europhys. Lett.*, **30**, 191.

Farago, O. and Santangelo, D. (2005). Pore formation in flactuating membrane. *J. Chem. Phys. 044901*, **122**, 044901.

Fattal, E., Youssef, M., Couvreur, P., and Andremont, A. (1989). Treatment of experimental salmonellosis in mice with ampicillin-bound nanoparticles. *Antimicrob Agents Chemother.*, **33**.

Fowler, S. D., Brown, W. J., Warfel, J., and Greenspan, P. (1987). Use of nile red for the rapid in situ quantitation of lipids on thin-layer chromatograms. *Journal of Lipid Research*, **28**.

Fredrickson, G. H., Ganesan, V., and Drolet, F. (2002). Field-theoretic computer simulation methods for polymers and complex fluids. *Macromolecules*, **35**, 16–39.

Gentilini, C., Evangelista, F., Rudolf, P., Franchi, P., Lucarini, M., and L.Pasquato (2008). Water-soluble gold nanoparticles protected by fluorinated amphiphilic thiolates. *J. Am. Chem. Soc.*, **46**(130), 15678–15682.

G.Gonnella, Orlandini, E., and Yeomans, J. (1997). Spinodal decomposition to a lamellar phase: Effects of hydrodynamic flow. *Phys. Rev. Lett.*, **78**, 1695.

Groot, R. D. and Warren, P. B. (1997). Dissipative particle dynamics: Bridging the gap between atomistic and mesoscopic simulation. *J. Chem. Phys.*, **107**(11), 4423.

Helfand, E. and Tagami, Y. (1971). Theory of the interface between immiscible polymer ii. *J. Chem. Phys.*, **56**(7), 3592.

Helfrich, W. (1978). Steric interaction of fluid membranes in multilayer systems. *Z. Naturforsch*, **33a**, 305.

Hömberg, M. (2008). Ein vergröbertes modell zur simulation von lipidmembranen. *Göttingen*.

Israelachvili, J. N. (1998). Intermolecular and surface forces. *Academic Press London*.

Jackson, A. M., Myerson, J. W., and Stellacci, F. (2004). Spontaneous assembly of sub-nanometre ordered domains in the ligand shell of monolayer protected nanoparticle. *Nature Materials*, **3**, 330–336.

Jin, W., Xu, P., Zhan, Y., Shen, Y., Kirk, E. A. V., Alexander, B., Murdoch, W. J., Liu, L., and Isaak, D. D. (2007). Degradable cisplatin-releasing core-shell nanogels from zwitterionic poly(β -aminoester)-graft-peg for cancer chemotherapy. *Drug Delivery*, **14**, 279–286.

Kelly, K. A., Nabeel, B., Rajesh, A., Sushma, G., Justin, B., Herlen, A., A., D. R., Umar, M., and Ralph, W. (2008). Targeted nanoparticles for imaging incipient pancreatic ductal adenocarcinoma. *PLoS Medicine*, **5**.

Kim, J., Oh, J., Milner, T. E., and Nelson, J. S. (2007). Imaging nanoparticle flow using magneto-motive optical doppler tomography. *Nanotechnology*, **18**(3), 035504 (6pp).

Koeleman, J. M. V. A. and Hoogerbrugge, P. J. (1993). An extended dissipative particle dynamics model. *Europhys. Lett.*, **21**, 363.

Krüger, C. (2008). Neue hybridmaterialien durch stöchiometrische funktionalisierung von nanopartikeln. *Marburg/Lahn*.

Lasic, D. D. (1994). Sterically stabilized vesicles.

Lomas, H., Canton, I., MacNeil, S., Du, J., Armes, S. P., Ryan, A. J., Lewis, A. L., and Battaglia, G. (2007). Biomimetic ph sensitive polymersomes for efficient dna encapsulation and delivery. *Advanced Materials*, page 4238.

Mark, J. E. (2007). Physical properties of polymers handbook. *Springer Cincinnati Ohio*.

Maskos, M. (2006). Influence of the solvent and the end groups on the morphology of cross-linked amphiphilic poly (1,2-butadiene)-b-poly(ethylene oxide) nanoparticles. *Polymer*, **47**, 1172–1178.

Meyer, H., Wittmer, J. P., Kreer, T., Beckrich, P., Johner, A., Farago, J., and Baschnagel, J. (2008). Static rouse modes and related quantities: Corrections to chain ideality in polymer melts. *Euro Phys. J. Lett.*, **26**, 25–33.

Müller, M. (1999). Miscibility behavior and single chain properties in polymer blends: a bond fluctuation model study. *Macromol. Theory Simul.*, **8**, 343 374.

Müller, M., Katsov, K., and Schick, M. (2006). Biological and synthetic membranes: What can be learned from a coarse-grained description? *Phys. Rep*, **434**, 113–176.

Orlandini, E. (2008). *Notes on the Lectures about Statistical Mechanics and Stochastic Processes.*

P. R. Mishra, N. K. J. (October 2003). Folate conjugated doxorubici-loaded membrane vesicles for improved cancer therapy. *Drug Delivery*, **10**, 277 – 282.

Pagonabarraga, I. and Frenkel, D. (2001). Dissipative particle dynamics for interacting systems. *J. Chem. Phys*, **115**, 5015.

Pastorino, C., Kree, T., Müller, M., and Binder, K. (2007). Comparison od dissipatice particle dynamics and langevin thermostats for out-of equilibrium simulations of polymeric system. *Phys. Rev. E*, **76**(2), 026706.

Sarkar, K. and Yang, H. (2008). Encapsulation and extended release of anti-cancer anastrozole by stealth nanoparticles. *Drug Delivery*, **15**, 343–346.

Shillcock, J. C. and Lipowsky, R. (2007). Visualiying soft matter: Mesoscopic simulations of membranes, vesicles and nanoparticles. *Biophys. Rev. and Lett.*, **2**, 33–55.

Singh, M., Ferdous, A. J., Branham, M., and Betageri., G. V. (1996). Pilosebaceous unit: anatomical considerations and drug delivery opportunitie. *Drug Delivery*, **3**, 289–304.

Torchilin, V. P. (2005). Recent advances with liposomes as pharmaceutical carriers. *Nature Reviews Drug Discovery*, **4**, 145 – 160.

Trominov, S. Y., Nies, E. L. F., and Michels, M. A. J. (2002). Thermodynamic consistency in dissipative particle dynamics simulations of strongly nonidel liquids and liquid mixtures. *J. Chem. Phy. Vol.*, **17**(20), 9384.

van Manen, H.-J. and Otto, C. (2007). Hybrid confocal raman fluorescence microscopy on single cells using semiconductor quantum dots. *Nano Letters*, **7**(6), 1631–1636.

Vuyst, E. D., Bock, M. D., Decrock, E., Moorhem, M. V., Naus, C., Mabilde, C., and Luc, L. (2008). In situ bipolar electroporation for localized cell loading with reporter dyes and investigating gap junctional coupling. *Biophysical Journal*, **94**, 469 – 479.

Wang, P., Jia, L., Sanders, B. G., and Kline, K. (2007). Liposomal or nanoparticle α-tea reduced 66cl-4 murine mammary cancer burden and metastasis. *Drug Delivery*, **14**, 497–505.

W.Müller, Koynov, K., Fischer, K., Pierrat, S., Schärtl, W., Basche, T., and Maskos, M. (2008). Hydrophobic shell of pb-b-peo vescicles. *Macromolecules*, **42**, 357–361.

Wu, D., Fredrickson, G. H., Carton, J. P., Ajdari, A., and L.Leibler (1995). Distribution of chain ends on a surface of polymer melt: Compensation effects and surface tension. *Journal of Polymer science*, **33**, 2373–2389.